The Dissertation Committee for Rohit Hegde
certifies that this is the approved version of the following dissertation:

Interactions and Quantum Hall Effects in Graphene Multilayers

Committee:

Allan Hugh MacDonald, Supervisor

James Chelikowsky

Gregory Fiete

Qian Niu

Zhen Yao

Interactions and Quantum Hall Effects in Graphene Multilayers

by

Rohit Hegde, B.S.

DISSERTATION

Presented to the Faculty of the Graduate School of

The University of Texas at Austin

in Partial Fulfillment

of the Requirements

for the Degree of

DOCTOR OF PHILOSOPHY

THE UNIVERSITY OF TEXAS AT AUSTIN

December 2013

Acknowledgments

Thank you, to Allan MacDonald, for your support and encouragement, guidance and teaching. I greatly appreciate your knowledge, understanding, enthusiasm, and wise presence. Thanks to James Chelikowsky, Greg Fiete, Qian Niu, and Zhen Yao for partaking in the dissertation and defense. Thanks, to group members past and present, and to colleagues, for your friendship, for teaching and sharing in learning, especially to Yasufumi Araki, Yafis Barlas, Rafi Bistritzer, Hua Chen, Ran Cheng, Victor Chua, Ashley da Silva, Karin Everschor-Sitte, Ion Garate, Charles Hanna, Hsian-Hsuan Hung, Insun Jo, Jeil Jung, Mehdi Kargarian, Guru Khalsa, Pantelis Lapas, Xiao Li, Maria Moura, Dmytro Pesin, Andreas Ruegg, Matthias Sitte, Inti Sodemann, Dagim Tilahun, John Tolsma, Maxim Trushin, James Wang-Kong Tse, Fengcheng Wu, Ming Xie, and Fan Zhang. Thanks to Becky Drake, Annie Harding, and Michele Landfield, for their assistance and support. Special thanks to Karin Everschor-Sitte and Matthias Sitte for proofreading parts of this thesis, and to Inti Sodemann, for many stimulating conversations. Thank you, to my parents and brother, for your love and support.

Interactions and Quantum Hall Effects in Graphene Multilayers

Publication No. _____

Rohit Hegde, Ph.D.
The University of Texas at Austin, 2013

Supervisor: Allan Hugh MacDonald

In a strong magnetic field, the psuedospin chirality of bilayer graphene's low energy bands results in degenerate, zero energy n=0 and n=1 Landau orbital states. In this thesis, we find that in addition to endowing states with energetic broadness disorder strongly mixes the zero energy orbitals of the lowest Landau level. We study the dependence of mixing and conductivity on inter-layer bias. Quantum Hall ferromagnetic states emerge when electronic interactions are included at the mean-field level. We study the character of ground states and quasiparticle excitations in the context of orbital degeneracy and in the presence of interactions with the filled Dirac sea of states. Lastly, we study the effect of interactions in ABA-stacked trilayer graphene, and discover a metal-insulator transition and a separate propensity to break mirror symmetry in certain areas of parameter space.

Table of Contents

List of Tables

List of Figures

Chapter 1

Introduction: Graphene

Many of the distinguishing electronic properties of graphene systems originate in the the psuedospin chirality of low-energy states. Here, we review low-energy models of single and bilayer graphene, highlight several phenomena emerging from chirality, and outline the calculations presented in this thesis.

Single layer graphene can be conceptualized as the arrangement of carbon atoms into a planar hexagonal lattice held together by sigma-bonded sp^2 orbitals, with one electron per atom occupying the p_z orbital. Often, the effective model of non-interacting electrons includes only the pi-bonded p_z orbitals of the two basis atoms per minimal unit cell. Applying Bloch's theorem results in a matrix Hamiltonian acting in the space of the two basis atoms (called A, and B) for every allowed reciprocal lattice vector $\vec{p}$:

$$H(\vec{p}) = -t \begin{pmatrix} 0 & \gamma(\vec{p}) \\ \gamma^*(\vec{p}) & 0 \end{pmatrix}, \quad \gamma(\vec{p}) = 1 + e^{i\vec{p}\cdot\vec{R}_1} + e^{i\vec{p}\cdot(\vec{R}_1+\vec{R}_2)} \tag{1.1}$$

where $t \approx 3eV$ is the π-bonding energy and the primitive lattice vectors expressed in terms of the inter carbon distance $a/\sqrt{3} = 1.42\text{Å}$ are

$$\vec{R}_1 = a\,\hat{x}, \quad \vec{R}_2 = -\frac{a}{2}\,\hat{x} + \frac{\sqrt{3}a}{2}\,\hat{y}. \tag{1.2}$$

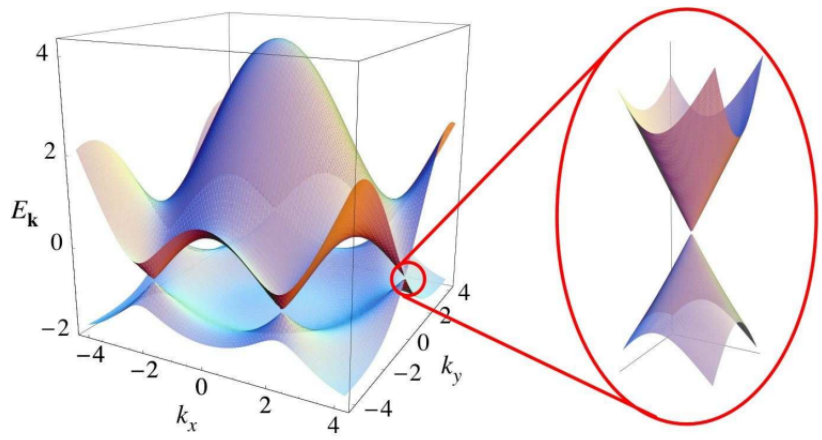

Figure 1.1: Adapted from [1]. The π-bands of single-layer graphene. The energy dispersion is linear for momenta near the Brillouin zone corners, the K and K' points.

The reciprocal lattice vectors defining the Brillouin zone are

$$\vec{G_1} = \frac{2\pi}{a}(\hat{x} + \frac{1}{\sqrt{3}}\,\hat{y}), \quad \vec{G_2} = \frac{4\pi}{\sqrt{3}a}\,\hat{y}. \tag{1.3}$$

The band energy is shown in Fig. 1.1. Given the large π-bandwidth of roughly 30000 Kelvin, it is useful to consider a low energy model valid for momenta close to the K and K' Brillouin zone corners which set the Fermi energy for a neutral graphene sheet.

Using $\vec{k}\cdot\vec{p}$ theory, the derivative effective continuum Hamiltonian is:

$$H(\vec{k}) = v\begin{pmatrix} 0 & \pi^\dagger \\ \pi & 0 \end{pmatrix} \tag{1.4}$$

where $v = \sqrt{3}/2ta$ is the Dirac velocity, $\pi = \xi k_x + ik_y$, with $\xi = (1, -1)$ for states near the (K,K') points, and $\vec{k}$ measures momentum from either the K or K' point. The energy of eigenstates of Eq(1.4) is $E = \pm vk$ and is independent

of the direction of $\vec{k}$, but the eigenstates

$$\Psi_{\pm} = \frac{1}{\sqrt{2}} \begin{pmatrix} 1 \\ \pm e^{i\theta_k} \end{pmatrix} \tag{1.5}$$

do depend on direction in a way that defines the notion of psuedospin chirality. It is clear from Eq(1.5) that the psuedospinor lies in the x-y plane, and that while adjusting θ_k from 0 to 2π, the direction of the psuedospinor also completes one full rotation. Correspondingly, states of single layer graphene are labeled by chirality index -1 or 1. The chiral nature of electronic states results in a Berry phase that profoundly affects electron dynamics. The Berry phase and corresponding Berry connection are properties of the momentum-dependent eigenstates and are given by

$$\gamma_n = \int_C d\vec{k} \cdot \vec{A}_{\vec{k}} \tag{1.6}$$

$$\vec{A}_{\vec{k}} = i\langle u_n(\vec{k}) | \vec{\nabla}_{\vec{k}} | u_n(\vec{k}) \rangle \tag{1.7}$$

where u_n are in general the Bloch eigenstates for a band n without the $e^{i\vec{k}\cdot\vec{r}}$ phase factor, and in this case correspond directly to $\Psi_{\pm}$. The Berry phase for electrons in graphene is π and can be calculated by adding to the Hamiltonian a gap term proportional to σ_z,

$$H_{gap} = \Delta \begin{pmatrix} 1 & 0 \\ 0 & -1 \end{pmatrix} \tag{1.8}$$

then evaluating Eq(1.7) for the resulting eigenstates and letting Δ go to zero. Before discussing the implication of the π Berry phase, we remark on the low-energy model of bilayer graphene.

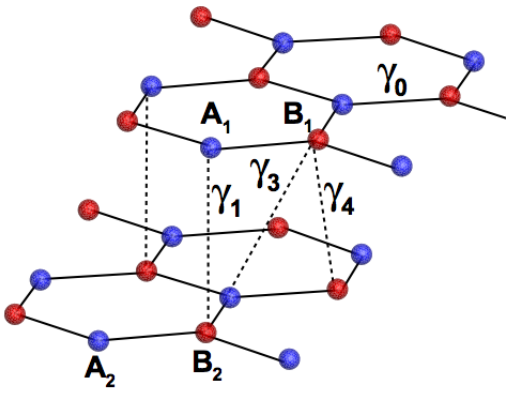

Figure 1.2: Adapted from [2]. Bilayer graphene comprises two bonded layers of graphene. The essential hoppings are γ_0 and γ_1, connecting intra- and inter-layer nearest neighbors. Further hoppings contribute effects like trigonal warping of the band structure.

Bilayer graphene comprises two bonded layers of graphene. There are four atoms per unit cell (Fig. 1.2), and the continuum Hamiltonian effective near the K and K' points acts on the basis (A_2, B_1, A_1, B_2).

$$H = \begin{pmatrix} 0 & 0 & 0 & v\pi^\dagger \\ 0 & 0 & v\pi & 0 \\ 0 & v\pi^\dagger & 0 & \gamma_1 \\ v\pi & 0 & \gamma_1 & 0 \end{pmatrix} \tag{1.9}$$

Two of the resultant four bands are pushed away in energy by $\pm\gamma_1$, where $\gamma_1 \approx 400meV$ is the inter-layer nearest neighbor bonding energy. An effective model for the two low-energy bands can be derived perturbatively [3] by expanding in inverse powers of γ_1. The lowest order Hamiltonian is quadratic in momentum:

$$H = \frac{1}{2m}\begin{pmatrix} 0 & \pi^{\dagger 2} \\ \pi^2 & 0 \end{pmatrix}, \quad m = v^2/2\gamma_1 \tag{1.10}$$

The band energy is $E = \pm\frac{k^2}{2m}$ and the eigenstates are

$$\Psi_{\pm} = \frac{1}{\sqrt{2}} \begin{pmatrix} 1 \\ \pm e^{2i\theta_k} \end{pmatrix} \tag{1.11}$$

Eigenstates of bilayer graphene's two-band model have chirality of two, and a corresponding Berry phase of 2π.

An important consequence of the nonzero Berry phases in single and bilayer graphene is the anomalous quantum Hall effect, characterized by the absence of a quantum Hall plateau at $\nu = 0$, and for single layer graphene, quantized Hall conductance of $(n + 1/2)\frac{e^2}{h}$ per spin and valley. Ordinarily, in semiconductor quantum well two-dimensional electron gases, the lowest electron-like Landau level has energy of half the cyclotron frequency, $E = \hbar\omega_C/2$, and the highest hole-like Landau level has $E = -\hbar\omega_c/2$, and there is a plateau of Hall conductance $\sigma_{xy} = 0$ near $\nu = 0$. In single and bilayer graphene, the psuedospin chirality of electrons leads to the existence of zero-energy Landau levels at $E = 0$ which preempt the formation of a $\nu = 0$ Hall plateau. The derivation of zero-energy levels will be presented in Chapter 2. The half-integer quantization observed [4] in graphene can be understood from a topological perspective. Usually, a magnetic field induces Landau levels which carry nonzero Chern number. In graphene, the π Berry phase contributes additionally to the Hall conductance, shifting the usual spectrum of plateaus by $\pm 1/2$.

Psuedospin chirality also plays an important role in determining the nature of interaction-induced symmetry breaking in bilayer graphene. It was shown [5] that within mean-field theory, the psuedospin that normally lies in

the x-y plane will point in the $\pm\hat{z}$ direction for momenta near the K and K' points, corresponding to a slight layer imbalance of charge. Considering both spins and valleys [6, 7], a landscape of SU(4) symmetry-broken states emerges, as charge can polarize to a different layer for each flavor of electron.

In Chapters 2 and 4 of this thesis, we investigate the physics of the chirality-protected zero-energy Landau levels of bilayer graphene. In Chapter 2, we study the disordered density of states and conductivity of bilayer graphene in a strong magnetic field, and show that even weak disorder can strongly mix the zero-energy levels. In Chapter 4, we study quantum Hall ferromagnetism in bilayer graphene near $\nu = 0$. We show that because the two zero-energy levels are of different orbital character, exchange interactions with the filled Dirac sea of states must be included to yield a particle-hole symmetric spectrum. In Chapter 3, we study ABA-stacked trilayer graphene, whose band structure comprises two single layer-like and four bilayer-like bands. We focus on interaction-induced mixing of bands of different chirality, which in this system is directly related to breaking of the lattice mirror symmetry.

Chapter 2

Disorder-Induced Landau Level Mixing in Bilayer Graphene

2.1 Introduction

Disorder is crucial to the emergence of the integer quantum Hall effect (IQHE) in two-dimensional electronic systems in strong magnetic fields. While topological theories of bulk [8, 9] and edge [10–12] dynamics provide essential insight into the novel types of order [13] underpinning the integer and fractional quantum Hall effects and into the related topological protection of the quantized Hall conductance, they cannot explain the broad plateaus in Hall conductance that constitute the key experimental signature of the IQHE [14]. In the canonical IQHE system, the quasi-two-dimensional electron gas (2DEG) systems found in quantum wells formed from GaAs/AlAs and related semiconductors, the role of disorder is twofold—it energetically broadens Landau levels and it localizes the majority of electronic states within each level.

Broadening lifts the massive degeneracy in energy of the electronic states of a Landau level, can be qualitatively captured by a perturbative treatment of disorder like the self-consistent Born approximation (SCBA) framework used in this chapter. In the SCBA broadening is related to the imagi-

nary part of the disorder-induced self-energy correction to the single-particle Green's function.

The SCBA also can also provide a theoretical description of two-particle properties such as charge polarization, current-current correlation, and longitudinal conductivity. For example the Kubo formula relates the conductivity to the current-current correlation function. For a 2DEG in the absence of a magnetic field, an infinite-ladder partial summation of the disorder perturbation theory Feynman diagrams is equivalent to semi-classical Boltzmann equation. Other diagrams capture quantum corrections to the semiclassical result. In particular, the maximally crossed ladder summation captures the influence of scattering-induced coherence between time-reversed scattering processes, leading to the weak localization that is commonly observed in the conductance of metals at low temperatures. In IQHE systems, the presence of a time-reversal symmetry-breaking magnetic field disrupts the aforementioned coherence and nullifies the weak-localization effect.

More generally, perturbative treatments of disorder cannot predict the strong Anderson-type localization present in IQHE systems. One can instead begin to understand localization from a simple, semi-classical perspective such as the percolation picture. Here, we think of the electron as moving in a circular cyclotron orbit with a radius of the magnetic length. In the presence of a non-uniform disorder potential, the center of the orbit (guiding center) drifts in a direction perpendicular to the potential's gradient. Consequently, guiding centers drift along equipotential contours and electrons become trapped near

local minima or maxima of the disorder potential. This simple picture explains why is is much easier to achieve strong localization effects when Landau levels have formed, compared to the case without a magnetic field. Only electronic states that have energy mid-way between the minima and maxima (states at the center of the Landau level) can extend over the system's area. The percolation picture underlies more rigorous quantum-mechanical models like the Chalker-Coddington model [15], which can explain quantum Hall plateaus.

Although it does not capture localization or the quantized Hall conductance, the SCBA can qualitatively account for longitudinal transport when the chemical potential lies near the center of a Landau level. It provides a good description of Landau level systems at higher temperatures when localization and the IQHE are disrupted by the inelastic scattering of electrons off thermally populated phonons.

In a strong magnetic field, bilayer graphene has the unusual property that $n = 0$ and $n = 1$ orbitals are degenerate in the eight-fold degenerate lowest $N = 0$ Landau level (LLL). In this chapter, we show use the SCBA to describe the unusual Landau level broadening and quantum transport physics that follows from this unusual property. In addition to inducing broadening, disorder in bilayer graphene can strongly mix $n = 0$ and $n = 1$ orbitals. In semiconductor quantum wells, this mixing is weak since each Landau level is separated from its neighbors by a large cyclotron energy. The degeneracy between orbitals follows from sub-lattice pseudo-spin chirality and quadratic dispersion of electronic states near charge neutrality point. When an elec-

tric field perpendicular to the layers is generated via top and back gates, the two orbitals split in energy, in proportion to the interlayer potential difference. We investigate the nature of level broadening and mixing in bilayer graphene's LLL and in the adjacent particle and hole type levels, allowing for this continuously tunable interlayer electric field. We present theories of the DC and AC conductivity as a function of Landau level filling and interlayer electric field.

2.2 Spectrum and Current

Like single-layer graphene, bilayer graphene is a gapless semiconductor. In a neutral bilayer, conduction and valence bands cross at the two *Dirac* points K and K' located at the corners of the honeycomb lattice Brillouin-zone. Although a Bernal stacked graphene bilayer contains four atoms per unit cell (A_1, B_1, A_2, B_2) and hence four π-bands, the p_z orbitals located at the A_1 and B_2 sites are coupled by interlayer hopping γ_1, and are consequently repelled from band-crossing energy. The low energy states at (A_2, B_1) couple to the higher energy ones via the intralayer nearest- neighbor hopping γ_0 process which vanishes at K and K'. Treating this coupling to second order in perturbation theory and integrating out the higher energy states results in a two-band low-energy Hamiltonian,

$$H = \frac{1}{2m}\begin{pmatrix} 0 & (k_x - ik_y)^2 \\ (k_x + ik_y)^2 & 0 \end{pmatrix} + \xi\Delta\left[\frac{1}{2}\begin{pmatrix} 1 & 0 \\ 0 & -1 \end{pmatrix} - \frac{1}{2m\gamma_1}\begin{pmatrix} \vec{k}^2 & 0 \\ 0 & -\vec{k}^2 \end{pmatrix}\right], \quad (2.1)$$

that is effective for momenta near the K ($\xi = 1$) and K' ($\xi = -1$) points and acts on pseudospinors (A_2, B_1) and (B_1, A_2) respectively. respectively [3]. Δ is the interlayer potential controlled by gates.

In the following we will neglect disorder coupling of states in different valleys and restrict our attention to valley K. The conductivities of valleys K and K' are identical. The influence of an external magnetic field can be included by substituting the velocity operator for the momentum, $\vec{\pi} = \vec{k} + (e/c)\vec{A}$. It is then easily verified that $a^\dagger = (2m\omega_C)^{-1/2}(\pi_x + i\pi_y)$ and its conjugate a satisfy $[a, a^\dagger] = 1$ and act as Landau level raising and lowering operators. The result is a Hamiltonian that operates on Landau orbital valued psuedospinors:

$$H = \omega_C \begin{pmatrix} 0 & a^2 \\ a^{\dagger 2} & 0 \end{pmatrix} + \xi\Delta \left[\frac{1}{2} \begin{pmatrix} 1 & 0 \\ 0 & -1 \end{pmatrix} - \frac{\omega_C}{\gamma_1} \begin{pmatrix} aa^\dagger & 0 \\ 0 & -a^\dagger a \end{pmatrix} \right]. \tag{2.2}$$

The cyclotron frequency of electrons in bilayer graphene $\omega_C = eB/mc$ depends linearly on magnetic field strength as it does in a conventional 2DEG, in contrast to single-layer graphene, where it is proportional to $\sqrt{B}$. In a balanced bilayer ($\Delta = 0$), the zeroth and first Landau orbitals are degenerate, $E_0 = E_1 = 0$, since

$$\begin{pmatrix} 0 & a^2 \\ (a^\dagger)^2 & 0 \end{pmatrix} \begin{pmatrix} 0 \\ \phi_0 \end{pmatrix} = \begin{pmatrix} 0 & a^2 \\ (a^\dagger)^2 & 0 \end{pmatrix} \begin{pmatrix} 0 \\ \phi_1 \end{pmatrix} = 0. \tag{2.3}$$

Biasing lifts this degeneracy with a gap that depends on the potential difference and the cyclotron frequency. In evaluating the conductivity, we will consider states in the four Landau levels closest to the neutrality points. These states

and their energies are given by

$$\Psi_0 = \begin{pmatrix} 0 \\ \phi_0 \end{pmatrix}, \qquad E_0 = -\frac{\delta}{2}\gamma_1, \tag{2.4}$$

$$\Psi_1 = \begin{pmatrix} 0 \\ \phi_1 \end{pmatrix}, \qquad E_1 = -\frac{\delta}{2}\gamma_1 + \delta\omega_C, \tag{2.5}$$

$$\Psi_{2\pm} = \begin{pmatrix} \pm D\phi_0 \\ \sqrt{1-D^2}\phi_2 \end{pmatrix}, \quad E_{2\pm} = \frac{1}{2}\Big(\delta\omega_C \pm \sqrt{8\omega_C^2 + \delta^2\gamma_1^2 - 6\delta^2\gamma_1\omega_C + 9\delta^2\omega_C^2}\Big). \tag{2.6}$$

where we define $\delta = \xi\Delta/\gamma_1$ for convenience, and

$$D = \frac{2E_2 - 4\delta\omega_C + \delta\gamma_1}{\sqrt{(2E_2 - 4\delta\omega_C + \delta\gamma_1)^2 + 8\omega_C^2}}. \tag{2.7}$$

Above, the $\pm$ corresponds to particle or hole-like states, respectively. Using

$$c\frac{\partial}{\partial A_x} = e\frac{\partial}{\partial \pi_x}, \tag{2.8}$$

on Eq. (2.1), we obtain the physical current, which consists of a term off-diagonal in layer index and a diagonal component present only at finite bias:

$$J_x = -e\sqrt{\frac{2\omega_C}{m}}\left[\begin{pmatrix} 0 & a \\ a^\dagger & 0 \end{pmatrix} + \frac{\delta}{2}\begin{pmatrix} -a - a^\dagger & 0 \\ 0 & a + a^\dagger \end{pmatrix}\right]. \tag{2.9}$$

The non-vanishing matrix elements of the current operator are

$$\langle\Psi_1|J_x(\vec{q}=0)|\Psi_0\rangle = -e\sqrt{\frac{\omega_C}{m}}\left(\frac{\delta}{\sqrt{2}}\right), \tag{2.10}$$

$$\langle\Psi_{2\pm}|J_x(\vec{q}=0)|\Psi_1\rangle = -e\sqrt{\frac{\omega_C}{m}}\big(\pm\sqrt{2}D + \delta\sqrt{1-D^2}\big). \tag{2.11}$$

2.3 SCBA Theory of Ordinary Two-Dimensional Electron Gases

In this section, we review self-consistent Born approximation theory applied to the case of a disordered 2DEG in a strong magnetic field. When the

cyclotron energy is much greater than the disorder potential, mixing of Landau levels can be ignored, and the self-energy reveals a simple analytic form for the broadened spectral function. We introduce two equivalent derivations of the conductivity—the first follows the Kubo approach, requiring evaluation of the current-current correlation function, the second relates the conductivity to the polarization function.

The Hamiltonian for a 2DEG in a perpendicularly oriented magnetic field is:

$$H = \hbar\omega_C\left(a^\dagger a + \frac{1}{2}\right), \tag{2.12}$$

where $\omega_C = eB/(mc)$ is the cyclotron energy, and $a^\dagger$, a are Landau level raising and lowering operators. Fixing the vector potential to $\vec{A} = (B/2)(-y, x, 0)$ leads to a set of symmetric gauge wavefunctions as the solution of Eq. (2.12):

$$|n, m\rangle = \frac{(a^\dagger)^n (b^\dagger)^m}{\sqrt{n!m!}}|0, 0\rangle, \tag{2.13}$$

where the zero angular momentum state is

$$\phi_{0,0}(\vec{r}) = \langle\vec{r}|0, 0\rangle = \frac{1}{\sqrt{2\pi l^2}}\exp[-z\bar{z}/(4l^2)].$$

Here, $z = x + iy$ and $\bar{z} = x - iy$ give the holomorphic and anti-holomorphic components of the position, and $l = \sqrt{\hbar c/(eB)}$ is the magnetic length. In the symmetric gauge, the Landau level and guiding center raising operators are given by:

$$a^\dagger = \frac{1}{\sqrt{2}}\left(\frac{z}{2l} - 2l\frac{\partial}{\partial\bar{z}}\right), \tag{2.14}$$

$$b^\dagger = \frac{1}{\sqrt{2}}\left(\frac{\bar{z}}{2l} - 2l\frac{\partial}{\partial z}\right). \tag{2.15}$$

The matrix elements of plane waves in the symmetric gauge basis are

$$\langle n', m'| \exp(-i\vec{k}\cdot\vec{r})|n, m\rangle = e^{-|k|^2/2} G_{n',n}(\bar{k}) G_{m',m}(k), \tag{2.16}$$

where

$$G_{a,b}(k) = \sqrt{\frac{b!}{a!}}\left(\frac{-ik}{\sqrt{2}}\right)^{a-b} {L_b}^{a-b}(|k|^2/2) \tag{2.17}$$

with ${L_b}^{a-b}(x)$ the associated Laguerre polynomial. Useful properties of these matrix elements that follow from the Landau level algebra include [16]:

$$\bar{G}_{a,b}(k) = G_{b,a}(-k) = G_{a,b}(-\bar{k}), \tag{2.18a}$$

$$\sum_a G_{a,a}(k) = N_\Phi \delta_{k,0}, \tag{2.18b}$$

$$\sum_b G_{a,b}(k_1) G_{b,c}(k_2) = \exp(-\bar{k_1} k_2/2) G_{a,c}(k_1 + k_2), \tag{2.18c}$$

where $N_\Phi = BA/\Phi_0$ is the number of flux quanta present in the system.

We include disorder by adding to the Hamiltonian

$$H_{\text{disorder}} = \sum_{j=1}^{N_{\text{imp}}} \int d\vec{r}\rho(\vec{r}) u(\vec{r} - \vec{R}_j), \tag{2.19}$$

where $u(\vec{r})$ is a Gaussian impurity potential. In Fourier space

$$u(\vec{q}) = u_0 \exp(-\pi^2 d^2 |q|^2) \tag{2.20}$$

where d is a potential-range parameter. Following the usual procedure of uniformly averaging over spatial configurations of impurities results in disordered Green's functions that remain diagonal in Landau level index and independent of the angular momentum quantum number (see Fig. 2.1). It follows from the

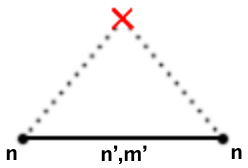

Figure 2.1: Leading-order self-energy diagram. The self-energy is diagonal in the Landau level index.

Dyson equation that the self-consistent Born approximate self-energy is (to second order in scattering off a single impurity and neglecting any uniform shift in energy at first order),

$$\Sigma_n(i\omega) = \frac{A|u_0|^2}{N_\Phi}\int \frac{d^2\vec{q}}{(2\pi)^2}\exp(-2\pi^2 d^2|q|^2) \times \sum_m \sum_{m',n'} \langle n,m|\exp(i\vec{q}\cdot\vec{r})|n',m'\rangle\langle n',m'|\exp(-i\vec{q}\cdot\vec{r})|n,m\rangle \mathcal{G}_{n'}(i\omega). \quad (2.21)$$

Using Eqns. (2.16) and (2.18), this expression reduces to

$$\Sigma_n(i\omega) = \sum_{n'} \frac{\Gamma^2_{nn'}}{4}\mathcal{G}_{n'}(i\omega) \quad (2.22)$$

with

$$\Gamma^2_{nn'} = \frac{4A|u_0|^2}{l^2}\int \frac{d^2\vec{q}}{(2\pi)^2}\exp(-|q|^2\lambda/2)|G_{n',n}(q)|^2, \quad (2.23)$$

where $\lambda = 1 + 4\pi^2 d^2/l^2$. For delta-function scattering, $\lambda = 1$, and the self-energy becomes independent of Landau level index:

$$\Gamma^2_{nn'} = 4N_\Phi|u_0|^2. \quad (2.24)$$

If the impurity potential is weak, we may neglect contributions to the self-energy of level n from other Landau levels, so that

$$\Sigma_n(i\omega) = \frac{\Gamma_{nn}^2}{4}\mathcal{G}_n(i\omega). \tag{2.25}$$

In this case, the zero-temperature disordered Green's function (Fig 2.2) is

$$\mathcal{G}_n^{(\mathrm{ret,adv})}(\omega) = \frac{2}{\omega - E_n \pm i[{\Gamma_{nn}}^2 - (\omega \mp i\eta - E_n)^2]^{1/2}}. \tag{2.26}$$

2.3.1 Universal DC Conductivity from the Kubo Formula

Here, we derive the DC conductivity of a delta-function disordered parabolic 2DEG in a quantizing magnetic field from the Kubo formula. Starting from the Hamiltonian (2.12), the component of the current operator in the x-direction is

$$j_x = -\frac{\partial H}{\partial A_x} = e\sqrt{\frac{\omega_C}{2m}}(a^\dagger + a). \tag{2.27}$$

For a Fermi energy lying in the n-th Landau level, it follows that the zero- temperature DC limit of the current-current correlation function includes Green's functions of levels $n-1$, n, and $n+1$. As in the case without a magnetic field, delta-function scatterers impart no vertex correction to the current operator [17]. In the SCBA this implies that the correction due to performing the particle-hole ladder diagram sum vanishes and the the current-current correlation is simply given by the bare loop diagram. In the Matsubara representation

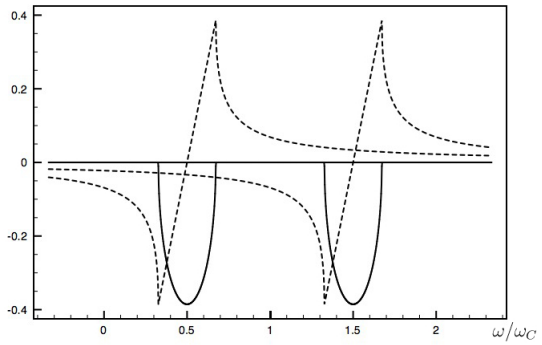

(a) Delta-function disorder.

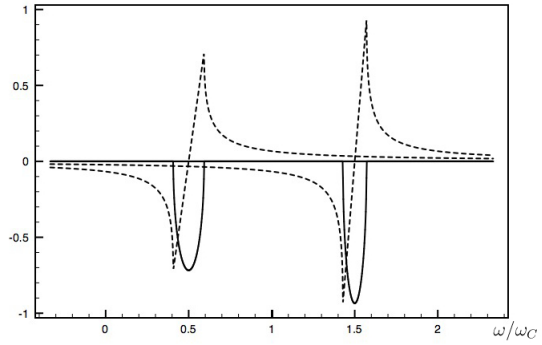

(b) Gaussian disorder with $d = l/4$.

Figure 2.2: Real (dashed) and imaginary (solid) parts of the retarded, disordered Green's function for (a) delta-function disorder and (b) Gaussian disorder with $d = l/4$. The imaginary part reveals the ellipsoidal broadening that is characteristic of the SCBA in a magnetic field.

we find that:

$$\Pi(\vec{q}=0,i\omega) = -e^2\frac{\omega_C}{2m}\frac{1}{\beta 2\pi l^2} \times \sum_{ik_n}\big[(n+1)(\mathcal{G}_n(ik_n)\mathcal{G}_{n+1}(ik_n+i\omega)+\mathcal{G}_{n+1}(ik_n)\mathcal{G}_n(ik_n+i\omega)) + n(\mathcal{G}_n(ik_n)\mathcal{G}_{n-1}(ik_n+i\omega)+\mathcal{G}_{n-1}(ik_n)\mathcal{G}_n(ik_n+i\omega))\big]. \quad (2.28)$$

From the Kubo formula for the conductivity,

$$\sigma(\omega) = -\frac{\operatorname{Im}\Pi(\vec{q}=0,\omega)}{\omega}, \quad (2.29)$$

the low-temperature, DC conductivity emerges from Eq. (2.28) by analytically continuing, then taking the low-frequency limit of the resultant, and finally reintroducing $\hbar$:

$$\sigma = e^2\frac{\omega_C^2}{2\hbar\pi^2}\operatorname{Im}\mathcal{G}_n(\mu)\big[(n+1)\operatorname{Im}\mathcal{G}_{n+1}(\mu)+n\operatorname{Im}\mathcal{G}_{n-1}(\mu)\big]. \quad (2.30)$$

For weak disorder, the Landau level width is much smaller than cyclotron energy, and we may expand

$$\operatorname{Im}\mathcal{G}_{n\pm1}(\mu) \approx \frac{\operatorname{Im}\Sigma_{n\pm1}(\mu)}{(E_{n\pm1}-\mu)^2} \approx \frac{\operatorname{Im}\Sigma_{n\pm1}(\mu)}{\omega_C^2} = \frac{\operatorname{Im}\Sigma_n(\mu)}{\omega_C^2}, \quad (2.31)$$

where the last equality follows from the fact the for delta-function scatterers, the self-energy is independent of Landau level index. Then, the DC conductivity is (see Fig. 2.3)

$$\sigma = \left(n+\frac{1}{2}\right)\frac{e^2}{\hbar\pi^2}\left[\frac{(\operatorname{Im}\Sigma_n(\mu))^2}{(\mu-E_n+\operatorname{Re}\Sigma_n(\mu))^2+(\operatorname{Im}\Sigma_n(\mu))^2}\right]. \quad (2.32)$$

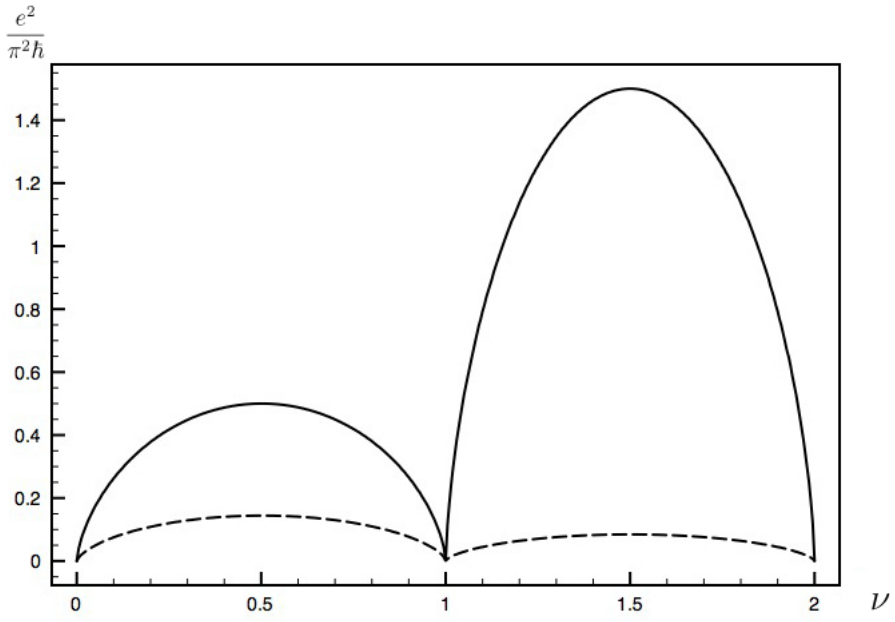

Figure 2.3: The DC conductivity as a function of Landau level filling factor ν, for delta-function disorder (solid) and gaussian disorder (dashed). At $\nu \equiv 1$, the chemical potential lies in a gap and the conductivity vanishes.

When μ is at the center of the n-th Landau level, the term in brackets will equal unity, resulting in a maximum-per-spin DC conductivity of

$$\sigma = \left(n + \frac{1}{2}\right)\frac{e^2}{\pi^2\hbar}. \tag{2.33}$$

This value is universal in that it depends only on the Landau level index, and is independent of cyclotron frequency and disorder strength.

2.3.2 Polarization

The polarization function that fulfills the Ward identity includes the ladder vertex correction commensurate with the approximation of the self-

energy outlined above. We assume a Fermi energy in the lowest Landau level and truncate the Hilbert space to include only that level. Then, the polarization function in the Matsubara frequency domain is [18]

$$\chi(\vec{q}, i\omega) = \frac{-1}{2\pi l^2 \beta} \sum_{\epsilon_n} \frac{\exp(-|q|^2 l^2/2)\mathcal{G}_0(\epsilon_n)\mathcal{G}_0(\epsilon_n + i\omega)}{1 - \exp[-|q|^2 l^2/(2\lambda)](\Gamma^2/4)\mathcal{G}_0(\epsilon_n)\mathcal{G}_0(\epsilon_n + i\omega)}. \quad (2.34)$$

The conductivity response to a purely longitudinal electric field can be derived from the charge continuity equation, and is related to the polarization as follows:

$$\mathrm{Re}\,\sigma_{xx}(\omega) = -\lim_{q\to 0} \frac{\omega}{q^2}\,\mathrm{Im}\,\chi(q_x, \omega). \quad (2.35)$$

The imaginary component of the diffusive polarization function, Eq. (2.34), which is quadratic in q for small q, yields a finite DC conductivity for a partially filled Landau level. Taking this limit of the polarization provides an alternative strategy for calculating the longitudinal conductivity. With this approach their is no substantial additional complication for the case in which the disorder potential has a finite range.

2.4 SCBA Treatment of Disorder in Bilayer Graphene

2.4.1 Disorder Broadening and Mixing

We model disorder with an intermediate-range potential that does not scatter electrons that is smooth over the distance between neighboring carbon atoms so that inter-valley scattering can be neglected. We also assume only on-site disorder. The scattering potential is therefore diagonal in valley and

layer indices and specified in momentum space by,

$$V(\vec{q}) = U\ \delta_{\tau\tau'}\ \delta_{\sigma\sigma'}\ \exp(-\pi^2 d^2 |q|^2). \tag{2.36}$$

This corresponds to delta-function scattering in real space when the range parameter $d \to 0$. (Since we neglect inter-valley scattering we should interpret this limit as corresponding to d small compared to magnetic lengths but large compared to a lattice constant.) Without inter-valley scattering, the SCBA self-energy and disorder-averaged Green's function retain terms that are off-diagonal in Landau level index, with disorder coupling particle and hole states:

$$G = G_{00} + G_{11} + \sum_{n\geq 2}(G_{nn} + G_{n,-n} + G_{-n,n} + G_{-n,-n}). \tag{2.37}$$

The self-energy of each Landau level contains terms proportional to the Green's functions of every other Landau level:

$$\Sigma_{nn'} = \sum_{n_1,n_2} S_{nn'}^{n_1 n_2} G_{n_1 n_2}. \tag{2.38}$$

The coefficients of the form S_{nn}^{nn} quantify level broadening while all others represent level mixing. The self-energy of a parabolically dispersing 2DEG with delta-function scatterers is independent of Landau level index, implying equal broadening of all levels. In bilayer graphene, layer polarization of the $n = 0$ and $n = 1$ levels results in broadening enhanced by $\sqrt{2}$ relative to other levels. For a scattering potential of finite Gaussian width $\lambda > 1$, broadening

becomes level specific:

$$S_{00}^{00} = 4\pi^2 N_\Phi U^2 \frac{1}{\lambda}, \tag{2.39}$$

$$S_{11}^{11} = 4\pi^2 N_\Phi U^2 \left(\frac{2}{\lambda^3} - \frac{2}{\lambda^2} + \frac{1}{\lambda} \right), \tag{2.40}$$

$$S_{22}^{22} = 2\pi^2 N_\Phi U^2 \left(\frac{6}{\lambda^5} - \frac{12}{\lambda^4} + \frac{10}{\lambda^3} - \frac{4}{\lambda^2} + \frac{1}{\lambda} \right). \tag{2.41}$$

Landau level mixing term can be neglected when disorder is weak compared to Landau level separation. For this quantum limit we obtain an analytic expression for the Green's functions, characterized by the ellipsoidal broadening that is the hallmark of SCBA in a quantizing magnetic field:

$$G_{nn}^{(\mathrm{ret,adv})}(\omega) = \frac{2}{\omega - E_n \pm i[4S_{nn}^{nn} - (\omega \mp i\eta - E_n)^2]^{1/2}}. \tag{2.42}$$

We use the above expression as a seed for a numerical solution of the Green's functions in the presence of disorder-induced Landau level mixing. The resulting density of states (see Fig. 2.4) depends sensitively on inter-layer biasing. Without inter-layer bias, the $n = 0$ and $n = 1$ levels are degenerate and the mixing terms $S_{00}^{11} = S_{11}^{00}$ act to further broaden the levels at neutrality to twice the width of the $n = 2$ level. Finite biasing narrows and separates the $n = 0$ and $n = 1$ levels until a gap opens.

2.4.2 DC Conductivity

We first consider the DC conductivity of an undoped, unbiased bilayer in the presence of delta-function scatterers. In this simplifying case, the spectrum exhibits particle-hole symmetry, and the degenerate K and K' valleys

contribute equally to the conductivity. The current operator simplifies with the relevant matrix element given by

$$\langle \Psi_{2\pm} | J_x(\vec{q}=0) | \Psi_1 \rangle = \mp e \sqrt{\frac{\omega_C}{m}}. \tag{2.43}$$

From the Kubo formula, the universal contribution to the conductivity from a single valley is

$$\sigma = e^2 \frac{{\omega_C}^2}{\hbar \pi^2} \operatorname{Im} \mathcal{G}_1(\mu) \operatorname{Im}(\mathcal{G}_{22}(\mu) + \mathcal{G}_{-2,-2}(\mu) - \mathcal{G}_{2,-2}(\mu) - \mathcal{G}_{-2,2}(\mu)). \tag{2.44}$$

Given the particle-hole symmetric spectrum, we have $\Sigma_{22} = \Sigma_{-2,-2}$ and

$$\begin{pmatrix} \mathcal{G}_{22} & \mathcal{G}_{2,-2} \\ \mathcal{G}_{-2,2} & \mathcal{G}_{-2,-2} \end{pmatrix} = \frac{1}{(i\omega - \Sigma_{22})^2 - E_2^2 - \Sigma_{2,-2}^2} \begin{pmatrix} i\omega + E_2 - \Sigma_{22} & \Sigma_{2,-2} \\ \Sigma_{2,-2} & i\omega - E_2 - \Sigma_{22} \end{pmatrix}. \tag{2.45}$$

Upon analytic continuation to zero frequency,

$$(\mathcal{G}_{22} + \mathcal{G}_{-2,-2} - \mathcal{G}_{2,-2} - \mathcal{G}_{-2,2}) = \frac{-2\Sigma_{22} - 2\Sigma_{2,-2}}{\Sigma_{22}^2 - \Sigma_{2,-2}^2 - E_2^2} \approx 2\frac{\Sigma_{22} + \Sigma_{2,-2}}{E_2^2} = \frac{2{\Sigma_{11}}^2}{E_2}, \tag{2.46}$$

where the last equality follows from $S_{22}^{11} = S_{2,-2}^{11} = S_{11}^{11}/2$, which is true only for delta-function scatterers. Including contributions from both valleys, the conductivity is

$$\sigma(\mu = 0; \delta = 0; \lambda = 1) = \frac{2e^2}{\pi^2 \hbar}. \tag{2.47}$$

2.4.3 Polarization Function

Owing to the near degeneracy of the $n = 0$ and $n = 1$ Landau levels, evaluation of the polarization function for fillings near neutrality requires inclusion of these levels' Green's functions. The polarization can be cast in matrix

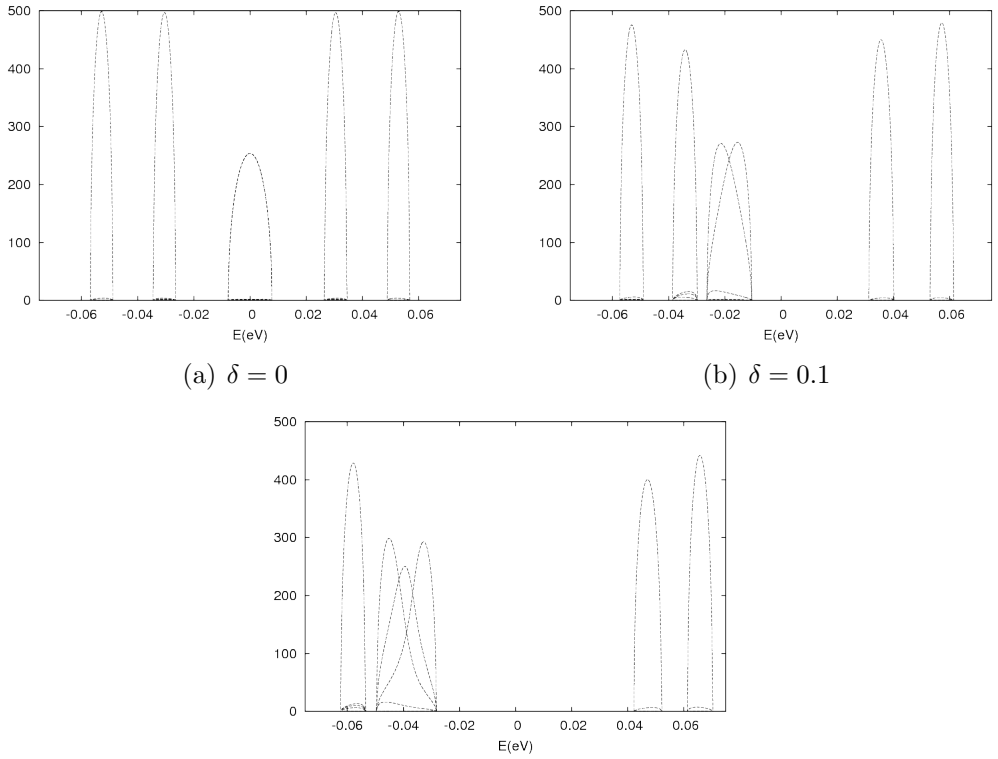

(a) $\delta = 0$

(b) $\delta = 0.1$

(c) $\delta = 0.2$

Figure 2.4: Spectral functions for zeroth, first, second, and third LL's of the K valley. (a)$\delta = 0$. With perfect degeneracy, mixing and broadening terms of the self-energy are identical, and combine to broaden the $N = 0$ Landau level to twice the width of the others. (b)$\delta = 0.1$. Orbital splitting between $n = 0$ and $n = 1$ is apparent, although the states are still strongly mixed. Note that the $n = 0, 1$ levels are more sensitive to the inter-layer bias potential than the $|n| > 2$ levels. (c)$\delta = 0.2$. The inter-layer bias is large enough that $n = 0$, $n = 1$, and $N = -2$ levels overlap.

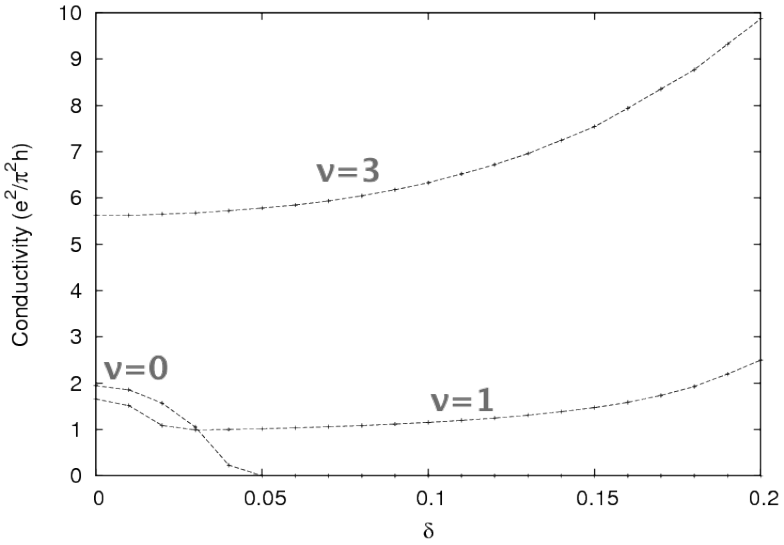

Figure 2.5: The DC conductivity as a function of δ for $\nu = 0, 1, 3$. For $\nu = 0$, a strong bias opens a gap between the $n = 0$ and $n = 1$ orbitals and the conductivity falls to zero.

form, where each matrix index α is a composite index specifying the Green's function at the top and bottom of the polarization loop (see Tab. 2.1). The number-conserving diffusion ladder is solved through matrix inversion. The full polarization function is

$$\chi(\vec{q}, i\omega) = \chi_0(\vec{q}, i\omega) + \frac{1}{2\pi\beta} \sum_{\epsilon_n} \exp(-|k|^2/2) L_\alpha T^{\alpha\beta}(\vec{q}) R_\beta, \tag{2.48}$$

where we have defined

$$L_\alpha = G_{\alpha_B, \alpha_T}(\bar{q}) \mathcal{G}_{\alpha_T}(\epsilon_n) \mathcal{G}_{\alpha_B}(\epsilon_n + i\omega), \tag{2.49}$$

$$R_\beta = G_{\beta_T, \beta_B}(-\bar{q}) \mathcal{G}_{\beta_T}(\epsilon_n) \mathcal{G}_{\beta_B}(\epsilon_n + i\omega). \tag{2.50}$$

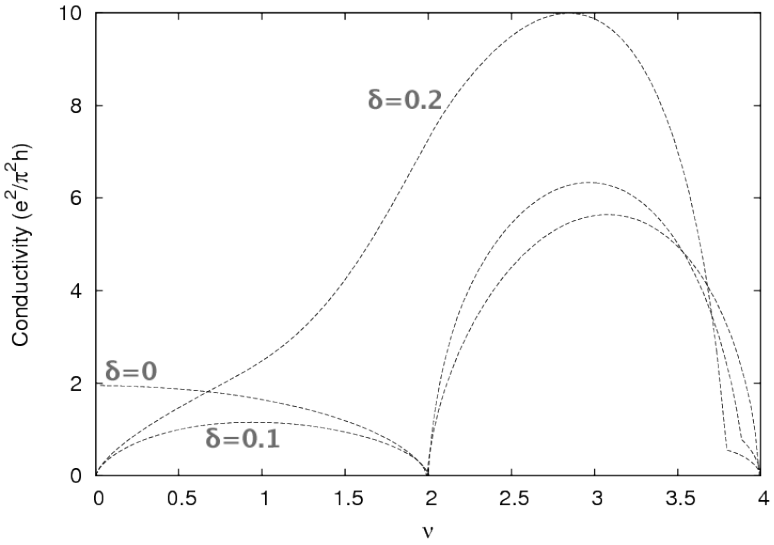

Figure 2.6: The DC conductivity as a function of ν for $\delta = 0, 0.1, 0.2$. The conductivity remains finite at $\nu = 1$ because the $n = 0$ and $n = 1$ orbitals are partially filled.

Furthermore, the diffusion ladder piece is given by

$$T^{\alpha\beta} = W_{\gamma}{}^{\alpha}[(1 - A)^{-1}]^{\gamma\beta}, \tag{2.51}$$

$$A^{\alpha\beta} = W^{\alpha\beta}\mathcal{G}_{\beta_T}(\epsilon_n)\mathcal{G}_{\beta_B}(\epsilon_n + i\omega), \tag{2.52}$$

and $W^{\alpha\beta}(\vec{q})$ is the matrix element for scattering between the four states labeled by α and β:

$$W^{\alpha\beta}(\vec{q}) = \frac{A|u_0|^2}{l^2}\int \frac{d^2\vec{k}}{(2\pi)^2}\exp[(|k|^2 - \bar{q}k + q\bar{k})/2]G_{\alpha_T,\beta_T}(-\bar{k})\bar{G}_{\alpha_B,\beta_B}(-\bar{k}). \tag{2.53}$$

The conductivity can be calculated from the polarization function as explained above in the ordinary two-dimensional electron gas case.

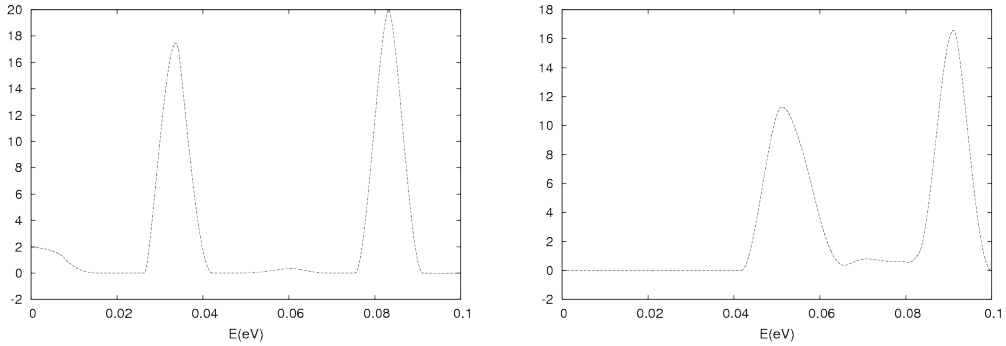

(a) $\delta = 0$ (b) $\delta = 0.1$

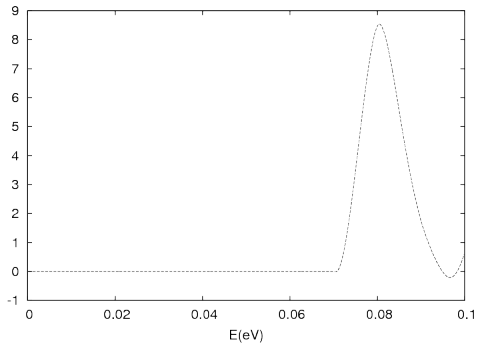

(c) $\delta = 0.2$

Figure 2.7: The AC conductivity at $\nu = 0$ displays various cyclotron resonances for (a) $\delta = 0$, (b) $\delta = 0.1$, and (c) $\delta = 0.2$.

α	α_T	α_B
0	0	0
1	0	1
2	1	0
3	1	1

Table 2.1: Composite Green's function index.

2.5 Discussion

The numerical results we have obtained for the density-of-states and the longitudinal conductivity highlight a number of interesting trends in the filling factor ν and inter-layer potential δ dependence of the electronic structure of bilayer graphene. Comparing panels a) and b) in Fig. 2.4 we see that the $n = 0, 1$ Landau levels are much more sensitive to a potential difference between the layers than Landau levels further from the Dirac point. This distinction is easy to understand, because the $n = 0, 1$ layers are already localized in a single-layer even in the absence of a potential difference, wheres the more remote Landau levels are partitioned equally between the two layers. A leading effect of a potential difference between the two-layers therefore appears at second order for $|n| \geq 2$, whereas the influence on the $n = 0, 1$ Landau levels appears at first order. The energy of the $n = 0, 1$ levels is therefore shifted rapidly toward the more remote valence band levels for one valley and toward the remote conduction band levels in the other valley. As we see in panel c) for stronger inter-layer bias potentials the $n = 0, 1$ levels are very strongly mixed with $|n| \geq 2$ levels for stronger δ. The stark difference in the influence of disorder between the weak and strong δ cases can be associated with the fact that the Landau level spacing near neutrality in the absence of disorder is strongly reduced by a finite value of δ.

Note that Fig. 2.4 plots the density-of-states for valley K. The density-of-states for valley K' differs by a change in sign of energy because an inter-layer potential which shifts $n = 0, 1$ states down in energy for one valley,

always shifts it up in energy in the other valley. It follows that the chemical potential at neutrality ($\nu = 0$) is always zero, and that the density of states at the Fermi level in a neutral system vanishes in panels (b) and (c).

The discussion below includes only disorder effects, and neglects interaction effects which tend to favor large spin or valley polarizations. Because the Zeeman coupling strength in bilayer graphene is small compared to interaction and disorder energy scales, we can also neglect spin-splitting when interactions are neglected. For this reason, the filling factors in the discussion below are all filling factors per spin.

The δ dependence of the longitudinal conductivity is illustrated in Fig.2.5. For $\nu = 0$ the longitudinal conductivity decreases with δ and vanishes beyond the critical value at which the density-of-states vanishes at $E = 0$, which is close to $\delta = 0.05$. At larger values of δ the filling factor per spin for one valley is $\nu = 1$ and for the other valley is $\nu = -1$. When the Fermi level is in the gap between the occupied $n = 0, 1$ states of one valley and the empty $n = 0, 1$ states of the other valley, both the longitudinal and the total Hall conductivity vanish. For $\nu = 1$ the Fermi level lies in the middle of the $n = 0, 1$ levels of one of the two valleys. Because the $n = 0, 1$ splitting within a valley is small, and because large δ leads to small energy spacings relative to the the $n \geq 2$ levels, a gap will appear at the Fermi level in this case only if disorder is quite weak. Similarly for $\nu = 3$, integer quantum Hall effects are likely to emerge only when interactions play a role, and the longitudinal conductivity remains large in our calculations.

Fig. 2.6 shows the filling factor dependence of the longitudinal conductivity for a balanced bilayer ($\delta = 0$) and for weakly ($\delta = 0.1$) and strongly ($\delta = 0.2$) unbalanced bilayers. For $\nu = 0$ gaps between Landau levels occur at $\nu = 2$ and $\nu = 4$. As expected our calculation finds longitudinal conductivity at these filling factors when disorder is not too strong. For $\delta = 0.1$ vanishing longitudinal conductivity also appears at $\nu = 0$ as explained above. At a larger value of δ the gap at $\nu = 0$ only grows, as explained above, but the gap at $\nu = 2$ weakens because the energy separation between the $n = 0, 1$ and remote Landau levels is reduced.

Fig. 2.7 shows typical results for the *ac* longitudinal conductivity at neutrality. For a balanced systems the conductivity has a small intra-Landau-level peak whose zero-frequency limit is the *dc* conductivity, as well as inter-Landau-level peaks which satisfy the $\delta|n| = 1$ selection rule. For the unbalanced cases illustrated the intra-Landau-level peak is absent because the *dc* conductivity has vanished.

The results presented in this section apply only in very strongly disordered systems in which interactions do not play a role. Unfortunately, both interactions and disorder are often important in quantum Hall systems including graphene. It will be valuable in the future to account for how the results described in this section are modified by interactions. For integer filling factors and for relatively strongly disordered samples, it may be sufficient to treat interactions at the level of the Hartree-Fock approximation, which can be readily combined with the SCBA. Experimentally the role of electron-

electron interactions can be reduced by placing the graphene bilayer sheet in a three-dimensional high-κ dielectric environment.

The following two-sections present discussions of multi-layer graphene physics in which interactions are essential, but disorder is neglected. Disorder can always be reduced experimentally, at least at low temperatures, by preparing more perfect samples. Disorder is nevertheless relevant for the interpretation of many different experimental results.

Chapter 3

Mirror Symmetry-Breaking Metal in Phase Diagram of ABA Trilayer Graphene

3.1 Introduction

ABA trilayer graphene is distinguished by a mirror-plane-symmetric lattice engendering a complex electronic structure of one monolayer pair and one bilayer pair of bands at low-energy. Each set of bands is gapped and displaced in energy relative to the other by non-nearest-neighbor hoppings and on-site energy differences, resulting in metallic behavior without doping. Rather than opening a gap at neutrality as would occur in chirally stacked few-layer graphene, an applied potential difference between extremal layers breaks trilayer's mirror-plane symmetry and hybridizes its monolayer and bilayer bands, enhancing conductivity and, with trigonal warping terms, generating a septuplet of Dirac cones at each valley.

Mean field [5] and renormalization group treatments [6, 7, 19, 20] of electronic interactions in chirally stacked systems like AB bilayer and ABC trilayer graphenes expose the possibility of inter-layer charge transfer for each species of fermion, resulting in a landscape of SU(4) spin-valley symmetry-broken candidate ground states.

In this chapter, we show that ABA trilayer's mean field phase diagram possesses a richness commensurate with the complexity of its non-interacting bands. We predict a finite-coupling transition to an insulating phase that *preserves* mirror-plane symmetry. Interactions open a gap by renormalizing the single-particle couplings of the continuum model, reshaping and shifting bands such that the density of states vanishes at neutrality. We also find electron-like and hole-like metallic regions of the phase diagram in which the self-consistent Hartree-Fock approximation allows for and energetically favors a breaking of mirror-plane symmetry, suggesting the possibility of tunable SU(4) breaking in clean samples.

3.2 Non-Interacting Continuum Model

The mirror plane symmetry of an unbiased trilayer motivates transformation from the atomic site basis to one in which orbitals of the extremal layers are dimerized with their reflection counterparts [21]. Written in the new basis $(A_1 - A_3)/\sqrt{2}, (B_1 - B_3)/\sqrt{2}, (A_1 + A_3)/\sqrt{2}, B_2, A_2, (B_1 + B_3)/\sqrt{2}$, the continuum Hamiltonian effective near the K and K' points separates into

blocks of definite parity:

$$H = \begin{pmatrix} H_{\mathrm{ML}} & \Delta \\ \Delta & H_{\mathrm{BL}} \end{pmatrix}, \tag{3.1a}$$

$$H_{\mathrm{ML}} = \begin{pmatrix} -\gamma_2/2 & v\pi^\dagger \\ v\pi & -\gamma_5/2 + \delta \end{pmatrix}, \tag{3.1b}$$

$$H_{\mathrm{BL}} = \begin{pmatrix} \gamma_2/2 & \sqrt{2}v_3\pi & -\sqrt{2}v_4\pi^\dagger & v\pi^\dagger \\ \sqrt{2}v_3\pi^\dagger & 0 & v\pi & -\sqrt{2}v_4\pi \\ -\sqrt{2}v_4\pi & v\pi^\dagger & \delta & \sqrt{2}\gamma_1 \\ v\pi & -\sqrt{2}v_4\pi^\dagger & \sqrt{2}\gamma_1 & \gamma_5/2 + \delta \end{pmatrix}. \tag{3.1c}$$

The 2×2 block is odd under reflection and comprises a pair of $J = 1$ Dirac bands, while the 4×4 block, even under reflection, contains a $J = 2$ quartet of bands like those in bilayer graphene. In AB bilayer graphene, conduction and valence bands are of odd and even parity, respectively. Therefore, breaking of inversion symmetry as by a perpendicularly-oriented electric field hybridizes bands and opens a gap at neutrality. It is clear from the block structure of ABA trilayer that mirror- plane symmetry breaking manifests quite differently, mixing via Δ the monolayer and bilayer *sectors* rather than hybridizing bands within each sector. In fact, an effect of remote hoppings γ_2, γ_5, and δ is to open gaps within the chiral subsectors, while *preserving* mirror symmetry.

Since two of the four bilayer-like bands are separated from neutrality by an energy on the order of γ_1, it is constructive to consider an effective model that clearly reveals the character of the four low-energy bands. Following the perturbative Green's function method that yields the usual two- band chiral

model of bilayer graphene [3], we find the following four-band model of ABA:

$$H = \begin{pmatrix} \Delta_C - \gamma_2/2 & v\pi^\dagger & \Delta_{MP} & 0 \\ v\pi & \Delta_C - \gamma_5/2 + \delta & 0 & -\Delta_{MP} v/(\sqrt{2}\gamma_1)\pi^\dagger \\ \Delta_{MP} & 0 & \Delta_C + \gamma_2/2 - \pi^\dagger\pi(\Delta_C - \delta/2)v^2/\gamma_1^2 & -(\pi^\dagger)^2 v^2/(\sqrt{2}\gamma_1) \\ 0 & -\Delta_{MP} v/(\sqrt{2}\gamma_1)\pi & -\pi^2 v^2/(\sqrt{2}\gamma_1) & -2\Delta_C + \pi^\dagger\pi(\Delta_C/2 + \delta/2 + \gamma_5/4)v^2/\gamma_1^2 \end{pmatrix}. \tag{3.2}$$

In deriving Eq. (3.2), we have included the symmetry-breaking potential $\Delta_{MP} = (U_1 - U_3)/2$ generated by a perpendicular electric field and the symmetry-preserving $\Delta_C = (U_1 + U_3 - 2U_2)/6$ that accounts for charge transfer to the center layer, and though not directly controllable by gating, arises naturally in a mean-field theory of electronic interactions. For clarity of presentation, we have omitted the trigonal warping terms (v_3, v_4). Interestingly, the symmetry breaking Δ_{MP}, which is defined in terms of the on-site energies of the six-band model, generates in the four-band model a mirror-plane anti-symmetric hopping between B sites that is the counterpart to the mirror-plane symmetric v_4 trigonal warping term of Eq. (3.1).

The minimal tight-binding model retains only intra-layer and inter-layer nearest-neighbor hoppings v, γ_1 and results in ideal, semi-metallic$J = 1$ and $J = 2$ band pairs with band touching points coinciding at charge neutrality. The dispersion of this model including finite Δ_{MP} is

$$E_{\vec{p}} = \pm\Big\{(p^2 + \Delta_{MP}^2)(2 + p^2/\gamma_1^2) \pm \left[(p^2 + \Delta_{MP}^2)^2(p^2 + 2\gamma_1^2)^2 - 8\gamma_1^2(p^3 - p\Delta_{MP}^2)^2\right]^{1/2}\Big\}^{1/2}. \tag{3.3}$$

Above, the inner plus-minus corresponds to band pairs that are monolayer and bilayer like for small values of Δ_{MP}. The monolayer pair carries a gap

of $4\Delta_{MP}$, while the bilayer pair touch at the point $\vec{p} = 0$ and on the ring $p = \Delta_{MP}$.

A realistic model includes the remote hoppings γ_2 and γ_5 connecting extremal A and B sites respectively, and the parameter δ that accounts for the difference in on-site energy between the $B1, A2, B3$ sites and the remaining three sites coupled by γ_1. Evident in the diagonal part of Eq. (3.2), these three parameters open gaps within each chiral subsector, but also shift the energy of one sector relative to the other, resulting in a non-vanishing density of states at all energies. Choosing parameters appropriate for ABA graphene like those derived from a density functional theoretic calculation [22] results in two band crossings at low energy between the bilayer pair and the valence monolayer band. In the absence of trigonal warping, the crossing between the conduction bilayer and valence monolayer band is circular and constitutes the Fermi surface of the neutral system. The sign of the monolayer gap is such that the $(A_1 - A_3)/\sqrt{2}$ orbital is the larger component of the valence monolayer band. At $p = 0$, the conduction bilayer state lies entirely on the B_2 orbital, while the valence bilayer band comprises $(A_1 + A_3)/\sqrt{2}$. The $J = 2$ gap is large enough that this orbital polarization persists to the momenta where the bands cross. Consequently, when the symmetry breaking Δ_{MP} is nonzero, the valence bilayer band hybridizes much more strongly with the valence monolayer band than does the conduction bilayer band. It has been shown that in a full model including trigonal warping, sufficiently large mirror-plane symmetry breaking generates a septuplet of Dirac cones at the crossing between conduction bilayer

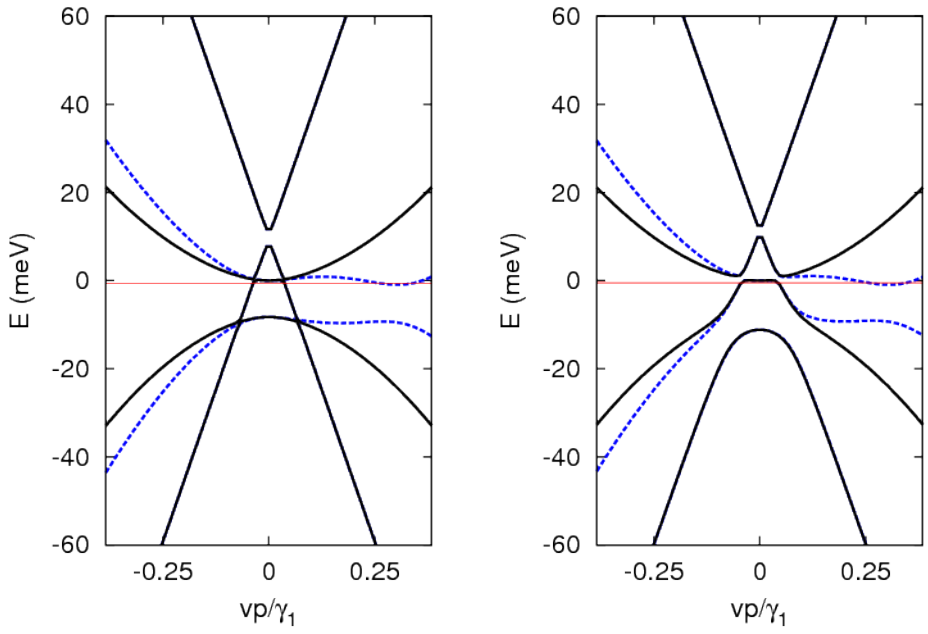

Figure 3.1: Left panel: The four low-energy bands of ABA graphene with hopping parameters derived from a density functional theoretic calculation. Solid (dashed) lines disperse in the p_x (p_y) direction. The Fermi level of a neutral trilayer crosses electron and hole bands. Right panel: Bands modified by a 15 meV potential difference between extremal layers. The valence monolayer band hybridizes more strongly with the valence bilayer band.

and valence monolayer bands [23, 24].

3.3 Mean Field Interactions

Mean field and renormalization group treatments of interactions among a single electron species expose the tendency toward inter-layer charge transfer and corresponding gap formation in chirally stacked systems like AB bilayer and ABC trilayer graphene. Electrons of different spin and valley may po-

larize to different layers, resulting in a landscape of SU(4) symmetry-broken candidate ground states. Since in ABA graphene layer polarization is not directly related to gap formation, we separately explore the potential of electronic interactions to induce layer polarization and to open a band gap between conduction and valence states. We consider the six-orbital model of spinless fermions described by seven tight-binding parameters [cf. Eq. (3.1)] plus a potential difference between extremal layers. We add electronic interactions governed by a layer-dependent Coulomb potential,

$$V_{\tau\tau'}(q) = \alpha \frac{\hbar v}{q} \exp(-q h_{\tau\tau'}), \tag{3.4}$$

where α is the effective fine-structure constant, and $h_{\tau\tau'} \in \{0, d, 2d\}$ is the $\hat{z}$ component of the displacement between orbitals τ and τ'. We find the self-consistent mean field ground state numerically by defining momentum states on a mesh, calculating the Hartree-Fock self-energy, then solving for the resultant bands, and iterating until the density matrix converges. Although incorporating a potential that is long-range and frequency-independent, our model accounts for the impact of screening phenomenologically by allowing α as a variational parameter. Small values of α correspond to significant dielectric screening, while $\alpha = 2.2$ reflects the unscreened limit.

The single-particle character of mean field theory allows the effect of interactions to be understood as a coupling-constant-dependent renormalization of the band Hamiltonian. The Hartree self-energy contributes a momentum-independent change to on-site energies, while Fock exchange allows

for momentum-dependent renormalization, inter-orbital coherence, and the breaking of symmetries originally present in the non-interacting model. Of particular importance to the present case of ABA graphene is renormalization of γ_2, γ_5, and δ, the parameters that sensitively determine the gaps of the monolayer and low-energy bilayer pairs, and set the energetic displacement of one pair with respect to the other. With increasing interaction strength, γ_2 becomes increasingly negative, while γ_5 remains largely unchanged, and δ becomes layer-dependent, growing in magnitude on the extremal layers, while decreasing on the middle layer. Overall, charge moves away from the middle layer and towards the A sites on the extremal layers, which are those not dimerized by γ_1. We find that across the phase diagram interactions of sufficient strength retune the continuum Hamiltonian such that a region of vanishing density of states appears in the spectrum. Above a critical coupling of $\alpha = 0.15$, an undoped trilayer is an insulator, as its Fermi energy lies in this conduction-valence gap (see Fig. 3.2). Importantly, this insulating phase does not break the lattice mirror-symmetry. As depicted in Fig. 3.3, the critical coupling increases with doping away from neutrality. Electron doping inhibits gap formation more strongly than does hole doping since electrons imbalance the population of the more strongly interacting bilayer pair.

3.4 Mirror-Symmetry Breaking

Although preserved in the insulating phase at neutrality, the mirror symmetry of the ABA lattice may break when doping places the system's Fermi

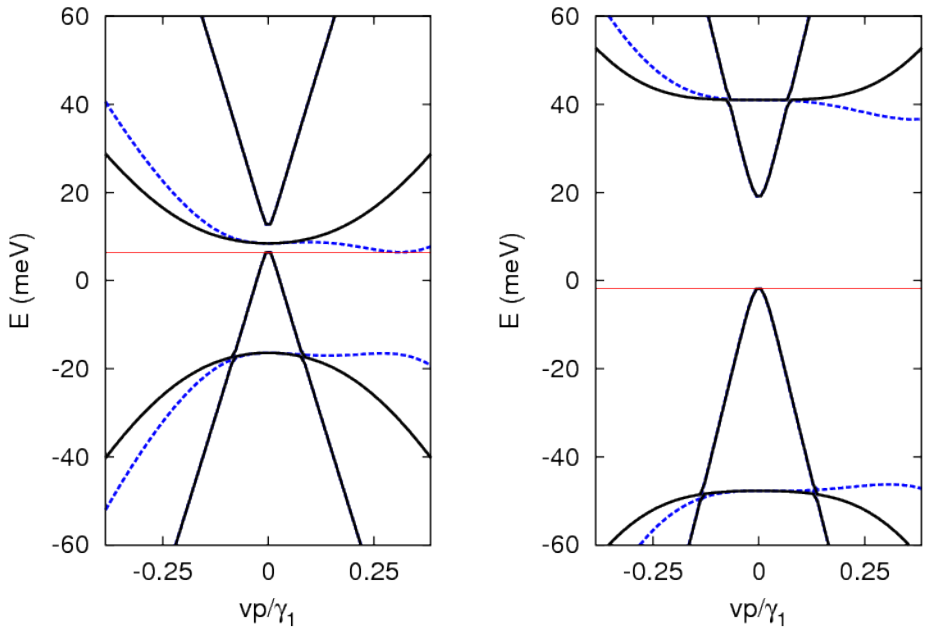

Figure 3.2: The Hartree-Fock renormalized bands of undoped ABA graphene shown at the critical coupling $\alpha = 0.16$ (left panel) and in the insulating phase, $\alpha = 0.5$ (right panel). Without doping, ground states are mirror-plane symmetric, and all bands remain distinctly monolayer- or bilayer-like.

energy near a crossing of monolayer and bilayer bands. The symmetry-broken metal phase is characterized by hybridization of the monolayer and bilayer sectors resulting in an avoided crossing near the Fermi energy (see Fig. 3.4). In the case of spinless and valleyless electrons, the density matrix also exhibits an imbalance of charge between extremal layers, with the metal carrying a slight layer polarization of up to 10^{-3} electrons per unit cell. The simplest type of mirror symmetry-breaking is the potential difference between extremal layers that was described in the non-interacting model. Interactions allow for more complex order since the self-energy can generally renormalize all eight of the

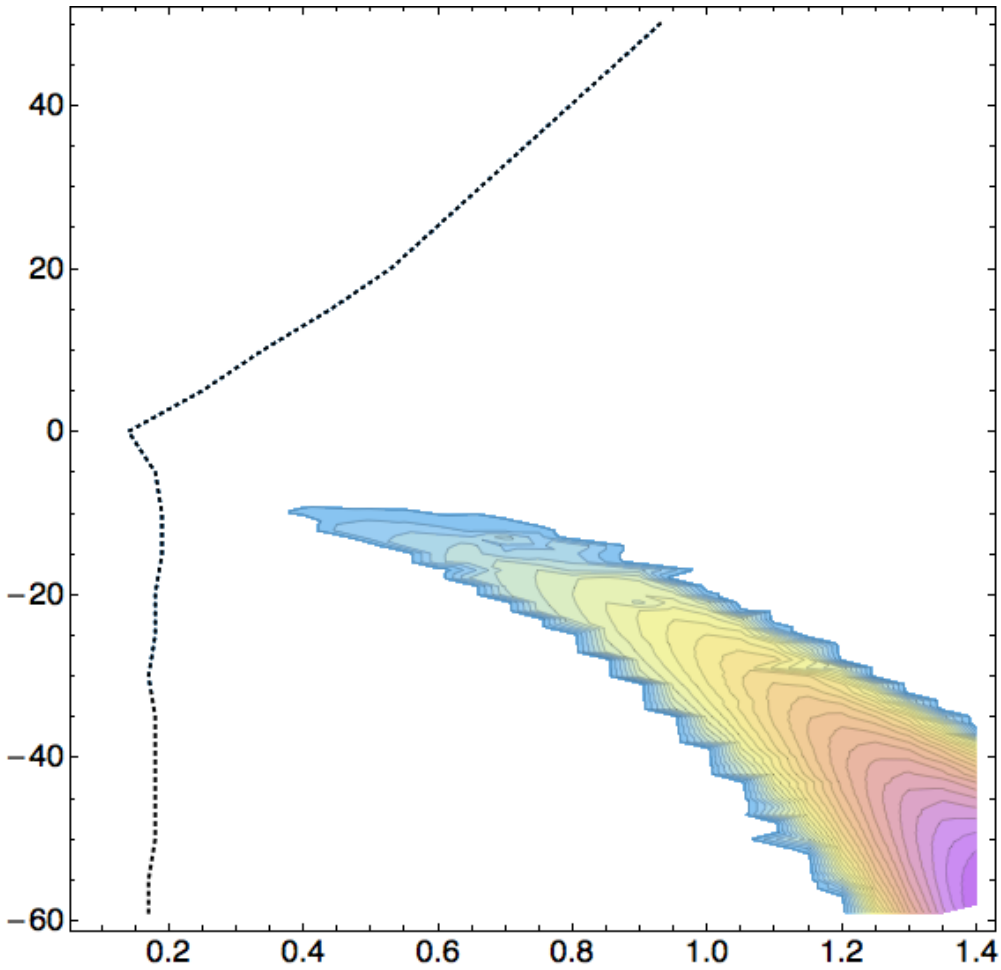

Figure 3.3: Mean-field phases as a function of interaction strength α and doping for spinless electrons of a single valley. The dashed lines bounds the trivial gapless phase to its left from the phases that exhibit a conduction-valence band gap. The colored region on the hole-doped side is the mirror-symmetry broken metal. The magnitude of layer-polarization in this state increases with doping and interaction strength. Here, we define the non-interacting model by finding the parameters that couple with weak interactions to reproduce the model parameters of [25].

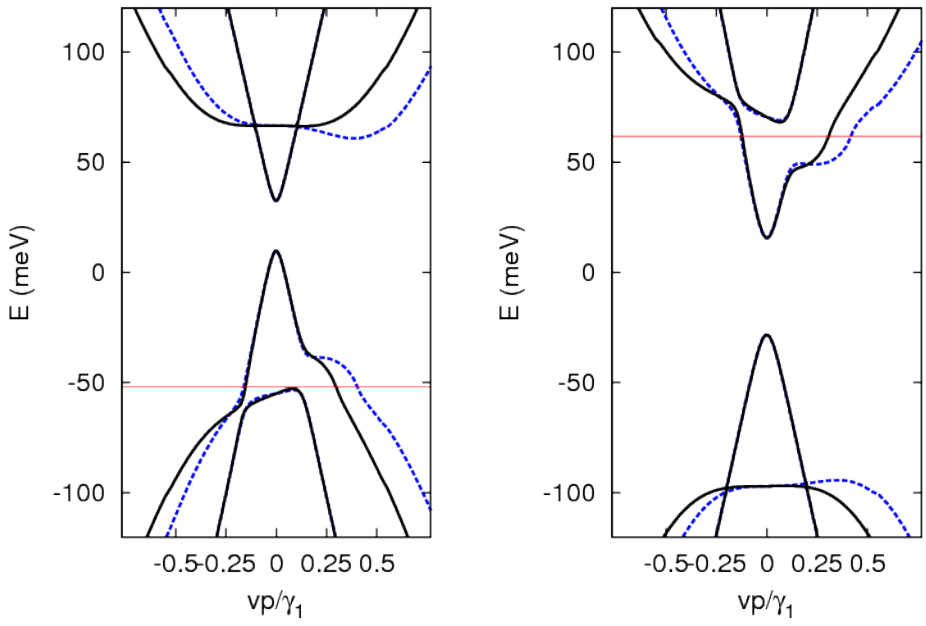

Figure 3.4: Mirror-plane symmetry-breaking states result when doping places the Fermi surface near the intersection of monolayer and bilayer bands. Left panel: Valence bands hybridize with hole doping of $\delta n = -10^{11}$ cm^{-2} and $\alpha = 0.7$. Right panel: Conduction bands hybridized with electron doping of $\delta n = 8 \cdot 10^{10}$ cm^{-2} and $\alpha = 0.85$.

Hamiltonian's symmetry-breaking matrix elements [in Eq. (3.1), Δ is a 2×4 matrix]. Some of these matrix elements contribute to asymmetrical hopping between orbitals, for example, the hopping between B_2 and B_3 may differ from the hopping between B_2 and B_1. Usually, all of the symmetry-breaking terms depend non-trivially on momentum, and in a particularly complex way when trigonal warping terms are included in the non-interacting Hamiltonian. Mirror-plane symmetry breaks in such a way that only the crossing nearest to the Fermi energy is avoided, leaving the seven other crossings largely intact.

In the layer-polarized state, charge transfers from the A site of one extremal layer to the A site of the other (the A sites are those not coupled to the middle layer by γ_1 hopping). Surprisingly, charge flows in the opposite direction between the extremal B sites. More charge is transferred between A sites, and so the sense in which the A sites are imbalanced determines the overall layer polarization direction. This asymmetrical charge transfer is endemic to ABA graphene, occurring not only in the spontaneously broken mirror-symmetry phase, but also in the normal phase when biased with a perpendicularly oriented electric field (see Fig. 3.5).

Within mean field theory, the instability towards layer polarization appears only at finite coupling of sufficient strength such that the system would be insulating if undoped. An increase in interaction coupling enlarges the gap between the low-energy bilayer bands more than it does the gap between the monolayer bands, thereby pushing the monolayer-bilayer crossings farther away from neutrality. Consequently, the density of doped electrons or holes needed to induce the layer-polarized state increases monotonically with coupling. In bilayer graphene, it is energetically favorable for electrons of different flavors to polarize to different layers so that the system is layer-balanced overall. Such a configuration has the advantage over a fully layer-polarized state of escaping the positive Hartree energy cost of layer-dependent Coulomb interactions, while the negative Fock energy remains unaltered due to the interaction's flavor-independence. With this in mind, we studied a two flavor model with an SU(2) invariant interaction and found that when the flavors polarize to

different layers, the mirror-symmetry broken state onsets at a slightly smaller value of coupling.

3.5 Discussion

Experiments on ABA-stacked trilayer graphene indicate that it is a metal at neutrality. A study of longitudinal transport of ABA on a boron nitride substrate in a magnetic field [25] found crossings between Landau levels of monolayer and bilayer type, and used the dependence of these crossings on ν and B to determine band parameters. In [26], metallic conductance was found in substrated and suspended samples with mobility of up to $\approx 2\times10^5 cm^2 V s^{-1}$.

It is likely then, that screening of electron-electron interactions is significant. The fact that within mean-field theory, the metal-insulator transition onsets only at finite coupling also suggests the possibility that screening may preempt the transition at realistic values of interaction coupling. An open question is whether screening would suppress the predicted tendency towards mirror-symmetry breaking in doped ABA graphene. This could be investigated within mean-field theory, by calculating the polarization function and replacing the bare Coulomb interaction with a statically screened potential.

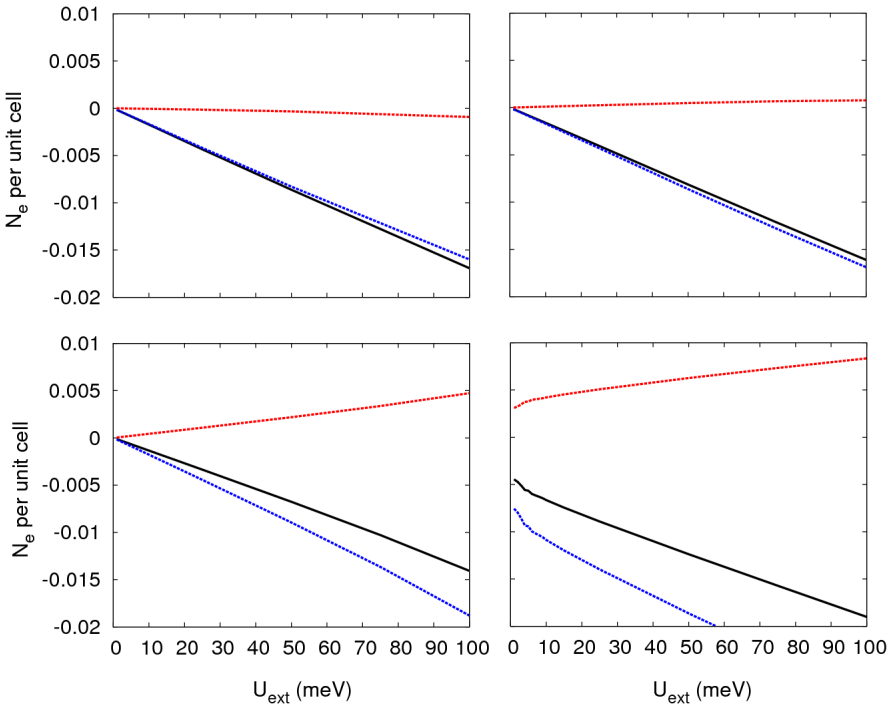

Figure 3.5: Charge imbalance between extremal layers in units of number of electrons per unit cell as a function of applied potential bias. The dashed (blue, red) lines are the sublattice ($n_{A1} - n_{A3}$, $n_{B1} - n_{B3}$) contributions to layer polarization while the solid black line is the sum of the two. Without interactions (top left) charge moves in the same direction on both sublattices. Charge polarizes asymmetrically when $\alpha = 0.3$ (top right) and $\alpha = 1$ (bottom left). With hole doping of $\delta n = -1.5 \cdot 10^{11}$ cm^{-2} (bottom right) charge transfer persists in the absence of external bias, signaling spontaneous breaking of mirror symmetry.

Chapter 4

The Vacuum Exchange Effect and Quantum Hall Ferromagnetism in Bilayer Graphene

4.1 Introduction

Subsequent to the experimental discovery [27] of the fractional quantum Hall effect and the development of a theoretical framework centered around Laughlin's correlated wavefunction [28], it was realized [29] that electron-electron interactions play an important role in the physics of integer-filled states. In a naive, non-interacting picture of the integer quantum Hall effect of spin-1/2 electrons, the first quantum Hall plateau would be observed near $\nu = 2$ (not $\nu = 1$) since both spin up and down states must be occupied in order to fully fill the lowest Landau level. Experiments on semiconductor quantum wells [30] revealed plateaus at $\nu = 1$ accompanied by quasiparticle gaps much larger than the Zeeman energy gap, suggesting an interaction effect. That interactions aquire prominence in quantum Hall effects follows naturally from the quenching of kinetic energy and associated macroscopic degeneracy of eigenstates within a Landau level. Mean-field treatment of interactions reveals a tendency toward broken symmetry ground states with Coulomb energy scale (e^2/ℓ) excitation gaps in integer-filled systems characterized by additional quantum numbers beyond the Landau level and guiding center numbers that

quantify an electron's orbital wavefunction. The name quantum Hall ferromagnetism (QHF) analogizes with the more familiar Stoner ferromagnetism of usual metals.

The rich phenomenology of QHF includes multi-component (e.g. spin and semiconductor valley) broken symmetry ground states supporting low-energy, neutral collective excitations that are generalizations of spin-waves in magnets. In some cases, charged excitations are simple quasiparticles, like a single quasielectron of spin down added to a full spin up Landau level. Often, QHF states support skyrmions [29, 31, 32], which are continuous deformations of the symmetry-breaking order parameter that carry topological charge (or winding number) *and* electrical charge. Bilayer quantum Hall systems, which comprise adjacent quantum wells separated by a potential barrier, support excitonic condensation [33, **?**] in the form of spontaneous interlayer coherence [34] between electrons and holes. Remarkable phenomenology ensues, like counterflow superfluidity, in which a drive current in one of the layers induces a dissipationless flow in the opposite direction in the other layer [35].

Quantum Hall effects are particularly interesting in graphene systems, where the non-trivial topologies of bands absent a magnetic field translate into novel Landau level spectra. The QHE can be understood to originate from incompressibilites at magnetic-field dependent densities [16], leading to dissipationless edge transport. From this perspective, the $\nu = 0$ (undoped) state of single-layer or bilayer graphene is not appropriately classified as a quantum Hall state, since its density equals zero irrespective of magnetic field

strength. Dissipationless edge transport is not guaranteed, and candidate ground states like the antiferromagnet that insulate both in bulk and at edge more closely resemble quantum spin Hall insulating states than traditional QH ones, despite the presence of a magnetic field. Recent studies [36–38] of QHF and FQH in single-layer graphene have underscored the importance of valley anisotropic interactions originating at the lattice-scale and breaking of SU(4) spin-valley symmetry.

The degenerate $n = 0$ and $n = 1$ orbitals of bilayer graphene's $N = 0$ Landau level add substantially to the complexity of ordering and correlation. At the mean-field level, the orbital-dependency of the Coloumb interaction implies that the orbital composition of the ground state depends strongly on the filling of the lowest Landau level. In usual semiconductor systems, states of $n = 1$ character are separated from $n = 0$ states by a large cyclotron energy, allowing for a perturbative treatment of Landau level mixing and preserving the orbital degree of freedom as a constant of motion. In contrast, bilayer graphene's orbital degeneracy allows for hybrid FQH states that contain inter-orbital correlations (one example is the $\nu = 2/5$ unprojected composite fermion wavefunction).

In this chapter, we explore the quantum Hall ferromagnetism of bilayer graphene, with a focus on the effect of the filled Dirac sea of states on dynamics in the $N = 0$ Landau level. That the exchange interaction with the Dirac sea has important consequences including restoring particle-hole symmetry has been exposed in recent papers [39, 40] by K. Shizuya. We examine the ground

states and its dependence on inter-layer biasing and intrinsic band particle-hole asymmetry.

4.2 Vacuum Exchange and Particle-Hole Symmetry in the $N = 0$ Landau Level

In this section, we demonstrate that when truncating the continuum Hamiltonian of interacting electrons in bilayer graphene to its lowest Landau level ($N = 0$), inclusion of the exchange-interaction with all filled states is required to yield the correct particle-hole symmetric spectrum. In sub-section 4.2.1 we calculate the vacuum exchange term in the context of the two-band model by regularizing the divergent interaction with the Dirac sea, paralleling a calculation by Shizuya for the four-band model of bilayer graphene. In sub-section 4.2.2 we rederive this result in a more general and rigourous way, by summing a convergent series. We explore the modification of vacuum exchange due to inter-layer bias and band particle-hole asymmetry in sub-section 4.2.3

The minimal model of interacting electrons in bilayer graphene consists of the two band continuum model plus Coulomb interactions:

$$H = H_0 + V, \tag{4.1a}$$

$$H_0 = \frac{1}{2m}\begin{pmatrix} 0 & {\pi^\dagger}^2 \\ \pi^2 & 0 \end{pmatrix}, \tag{4.1b}$$

$$V = \frac{1}{2A}\sum_{\vec{q}} v_{\vec{q}}\rho_{\vec{q}}\rho_{-\vec{q}}. \tag{4.1c}$$

The non-interacting chiral term H_0 describes conduction and valence bands dispersing with energy $E_{\vec{k}} = \pm k^2$ and is particle-hole symmetric. Inter-

changing particles with holes in V, which describes two-body interactions among electrons results in an identical interaction among holes plus a one-body Hartree-Fock potential generated by filling *all* eigenstates. The one-body term corresponds to interactions with a uniform charged background and can be safely discarded. Thus, we conclude that the full Hamiltonian, Eq(4.1a), is particle-hole symmetric.

We describe dynamics in the presence of a strong magnetic with Landau gauge eigenstates of H_0:

$$\Psi^{(K)}_{N,X} = \frac{1}{\sqrt{2}} \begin{pmatrix} \phi_{N-2,X} \\ \mathrm{sgn}(N)\phi_{N,X} \end{pmatrix}, |N| \geq 2 \tag{4.2a}$$

$$\Psi^{(K)}_{n,X} = \begin{pmatrix} 0 \\ \phi_{n,X} \end{pmatrix}, n = \{0, 1\} \tag{4.2b}$$

Here, states are of valley K, X is the guiding center index, $N = \{\pm 2, \pm 3, ... \pm \infty\}$ are the conduction and valence Landau levels, and $n = \{0, 1\}$ are the two degenerate, zero-energy orbitals that comprise the $N = 0$ lowest Landau level (see section 2.2). As usual, states of valley K' are obtained by interchanging the top with the bottom layer.

The interaction can be expressed in a compact form,

$$V = \frac{1}{2} \sum_{\alpha\beta\gamma\delta} v_{\alpha\beta\gamma\delta} c^\dagger_\alpha c^\dagger_\beta c_\gamma c_\delta, \tag{4.3}$$

where $\alpha = \{N_\alpha, X_\alpha, \tau_\alpha, \sigma_\alpha\}$ is a composite index specifying Landau level, guiding center, valley, and spin quantum numbers, and

$$v_{\alpha\beta\gamma\delta} = \frac{1}{A} \sum_{\vec{q}} \frac{2\pi e^2}{q} \langle \beta | e^{i\vec{q}\cdot\vec{r}} | \gamma \rangle \langle \alpha | e^{-i\vec{q}\cdot\vec{r}} | \delta \rangle \tag{4.4}$$

includes both the Coulomb potential and form factors.

Under a particle-hole transformation ($c^\dagger \to d, c \to d^\dagger$) the interaction becomes

$$V = \frac{1}{2}\sum_{\alpha\beta\gamma\delta} v_{\alpha\beta\gamma\delta} d^\dagger_\alpha d^\dagger_\beta d_\gamma d_\delta + \sum_{\alpha\beta\gamma} \left(v_{\alpha\gamma\gamma\beta} - v_{\alpha\gamma\beta\gamma}\right) d^\dagger_\alpha d_\beta. \tag{4.5}$$

The second term is the aforementioned Hartree-Fock potential generated by the filled states (γ), and can be discarded if the sum over γ is unrestricted. When the interaction is projected to the lowest Landau level, $n_\gamma \in \{0, 1\}$ and the Hartree-Fock potential becomes orbital-dependent, and therefore must be retained:

$$V = \frac{1}{2}{\sum_{\alpha\beta\gamma\delta}}' v_{\alpha\beta\gamma\delta} d^\dagger_\alpha d^\dagger_\beta d_\gamma d_\delta + \frac{e^2}{\ell}\sum_{\tau\sigma X}\left(\frac{3}{2}\sqrt{\frac{\pi}{2}}\, d^\dagger_{0,X,\tau,\sigma} d_{0,X,\tau,\sigma} + \frac{5}{4}\sqrt{\frac{\pi}{2}}\, d^\dagger_{1,X,\tau,\sigma} d_{1,X,\tau,\sigma}\right) \tag{4.6}$$

The prime over the first sum indicates restriction to the lowest Landau level. In the second term, and in the remainder of this section, the Hartree term is dropped as its constant, infinite energy shift is countered by charge neutrality. That the second term is nonzero and orbital-dependent implies that the spectrum for holes differs from the spectrum for electrons in the lowest Landau level. We show in the following that this artefact is remedied by adding the exchange potential generated by all filled ($N \leq -2$) states to the dynamics of $N = 0$ electrons:

$$V = \frac{1}{2}{\sum_{\alpha\beta\gamma\delta}}' v_{\alpha\beta\gamma\delta} c^\dagger_\alpha c^\dagger_\beta c_\gamma c_\delta - {\sum_{\alpha}}' \sum_{\beta\notin \mathrm{LLL}} v_{\alpha\beta\alpha\beta} c^\dagger_\alpha c_\alpha \tag{4.7}$$

4.2.1 Regularization of Exchange Interaction with Dirac Sea

The second term of Eq(4.7) quantifies the exchange potential generated by the infinite number of valence states comprising the Dirac sea (vacuum exchange). For either value of n_α, the summation of the interaction coefficient over N_β from -2 to $-\infty$ diverges. That an ultraviolet divergence might arise in the context of a low-energy effective field theory is unsurprising, and in this case the infinity can be absorbed in the renormalization of the chemical potential. The proper regularization scheme reveals itself when the Landau level dependence of the interaction coefficient is made explicit. In the following, only the Landau level quantum numbers are displayed since spin and valley indices are peripheral, and since the exchange potential is diagonal in guiding center index (which follows from spatial homogeneity of the Dirac sea):

$$H_{DS} = \frac{-1}{A}\sum_{\alpha}{}^{'}\sum_{N\geq 2}\frac{1}{2}\sum_{\vec{q}}\frac{2\pi e^2}{q}\langle n_\alpha|e^{-i\vec{q}\cdot\vec{r}}|N\rangle\langle N|e^{i\vec{q}\cdot\vec{r}}|n_\alpha\rangle. \tag{4.8}$$

Using the Landau level resolved identity ($\mathbb{I} = \sum_{N=0}^{\infty}|N\rangle\langle N|$), this becomes

$$H_{DS} = \frac{1}{A}\sum_{\alpha}{}^{'}\sum_{N\in\{0,1\}}\frac{1}{2}\sum_{\vec{q}}\frac{2\pi e^2}{q}\langle n_\alpha|e^{-i\vec{q}\cdot\vec{r}}|N\rangle\langle N|e^{i\vec{q}\cdot\vec{r}}|n_\alpha\rangle c_\alpha^\dagger c_\alpha - \frac{1}{A}\sum_{\vec{q}}\frac{2\pi e^2}{q}. \tag{4.9}$$

The second term is an ignorable constant, the first evaluates to:

$$H_{DS} = \frac{e^2}{\ell}\sum_{\tau\sigma X}\left(\frac{3}{4}\sqrt{\frac{\pi}{2}}\,c^\dagger_{0,X,\tau,\sigma}c_{0,X,\tau,\sigma} + \frac{5}{8}\sqrt{\frac{\pi}{2}}\,c^\dagger_{1,X,\tau,\sigma}c_{1,X,\tau,\sigma}\right) \tag{4.10}$$

In a sense, regularization recasts the negative exchange interaction with the infinite Dirac sea as a positive exchange interaction with the $n = \{0, 1\}$ sector

that is 'missing' from the Dirac sea. However it is crucial that the factor of 1/2 present in Eq(4.9) comes from the layer distribution of the Dirac sea, and so vacuum exchange does not truly represent intra-lowest Landau level interactions. Clearly, the vacuum exchange potential, Eq(4.10) is similar to the single particle potential acting on holes in the $N = 0$ Landau level expresed in Eq(4.6). In fact, it is easy to verify that adding the vacuum exchange potential to the electron-electron interaction term projected to $N = 0$ results in a Hamiltonian that is precisely particle-hole symmetric.

4.2.2 Summation of Convergent Series

The regularization method of the previous section is elegant and compact, but cannot be simply applied when important non-interacting terms like the one capturing inter-layer biasing are added to the band Hamiltonian. In the presence of such terms, the layer weighting of states becomes Landau level dependent,

$$\Psi_{\pm N,X} = \begin{pmatrix} A_{\pm N}\,\phi_{N-2,X} \\ B_{\pm N}\,\phi_{N,X} \end{pmatrix}, \quad |N| \geq 2, \tag{4.11}$$

and the identity 'trick' employed previously is no longer applicable. It is useful to consider a more general expression of the vacuum exchange potential. Irrespective of the precise structure of the Dirac sea, vacuum exchange imparts an infinite negative energy shift to both $n = 0$ and $n = 1$ orbital states, but

only the energy *difference* between these orbitals is physically important:

$$\begin{aligned}\Delta_{DS} &= \epsilon_{DS,1} - \epsilon_{DS,0} \\ &= \frac{-1}{A}\sum_{N=2}^{\infty}|B_{-N}|^2\sum_{\vec{q}}\frac{2\pi e^2}{q}\left[\langle N|e^{i\vec{q}\cdot\vec{r}}|1\rangle\langle 1|e^{-i\vec{q}\cdot\vec{r}}|N\rangle - \langle N|e^{i\vec{q}\cdot\vec{r}}|0\rangle\langle 0|e^{-i\vec{q}\cdot\vec{r}}|N\rangle\right] \\ &= -\sum_{N=2}^{\infty}|B_{-N}|^2\left(X_{N11N} - X_{N00N}\right) \quad (4.12)\end{aligned}$$

The plane wave matrix element can be reexpressed in terms of Landau level raising and lowering operators, so the energy difference due to a single filled level N is:

$$\begin{aligned}X_{N11N} - X_{N00N} = \\ e^2\int\frac{d\vec{q}\ell}{2\pi q}e^{-|q|^2\ell^2/2}[&\langle N|e^{\bar{w}a^\dagger}e^{-wa}|1\rangle\langle 1|e^{-\bar{w}a^\dagger}e^{wa}|N\rangle \\ &- \langle N|e^{\bar{w}a^\dagger}e^{-wa}|0\rangle\langle 0|e^{-\bar{w}a^\dagger}e^{wa}|N\rangle], \quad (4.13)\end{aligned}$$

where $w = \ell iq/\sqrt{2}$. The algebra of raising and lowering operators implies that

$$\begin{aligned}\langle N|e^{\bar{w}a^\dagger}e^{-wa}|1\rangle &= \langle N|e^{\bar{w}a^\dagger}|1\rangle - w\langle N|e^{\bar{w}a^\dagger}|0\rangle, \\ \langle 1|e^{-\bar{w}a^\dagger}e^{wa}|N\rangle &= \langle 1|e^{wa}|N\rangle - \bar{w}\langle 0|e^{wa}|N\rangle \quad (4.14)\end{aligned}$$

So,

$$\begin{aligned}X_{N11N} - X_{N00N} = \\ e^2\int\frac{d\vec{q}\ell}{2\pi q}e^{-|q|^2\ell^2/2}[&\langle N|e^{\bar{w}a^\dagger}|1\rangle\langle 1|e^{wa}|N\rangle + \left(|w|^2-1\right)\langle N|e^{\bar{w}a^\dagger}|0\rangle\langle 0|e^{wa}|N\rangle \\ &- w\langle N|e^{\bar{w}a^\dagger}|0\rangle\langle 1|e^{wa}|N\rangle - \bar{w}\langle N|e^{\bar{w}a^\dagger}|1\rangle\langle 0|e^{wa}|N\rangle]. \quad (4.15)\end{aligned}$$

Then, using

$$\langle N|e^{\bar{w}a^\dagger}|0\rangle = \frac{\bar{w}^N}{\sqrt{N!}}$$
$$\langle N|e^{\bar{w}a^\dagger}|1\rangle = N\frac{\bar{w}^{N-1}}{\sqrt{N!}}, \tag{4.16}$$

and performing the angular integration over θ_q yields

$$X_{N11N} - X_{N00N} = e^2 \int_0^\infty \frac{dq\ell}{N!} e^{-|q|^2\ell^2}[N^2|w|^{2(N-1)} + (|w|^2 - 1)|w|^{2N} - 2N|w|^{2N}]. \tag{4.17}$$

Finally, evaluating this integral gives

$$X_{N11N} - X_{N00N} = \frac{\Gamma(N - \frac{1}{2})}{\sqrt{32}N!}\frac{e^2}{\ell} \tag{4.18}$$

Clearly, this energy difference approaches zero in the limit that $N \to \infty$, and in fact, the summation of this term is convergent:

$$\frac{e^2}{\ell}\sum_{N=2}^{\infty}\frac{\Gamma(N - \frac{1}{2})}{\sqrt{32}N!} = \frac{1}{4}\sqrt{\frac{\pi}{2}}\frac{e^2}{\ell} \tag{4.19}$$

The advantage of this approach is that it allows for an expression for Δ_{DS} that can be evaluated numerically, for general B_N:

$$\Delta_{DS} = -\frac{e^2}{\ell}\sum_{N=2}^{\infty}|B_{-N}|^2\frac{\Gamma(N - \frac{1}{2})}{\sqrt{32}N!} \tag{4.20}$$

That the term $(X_{N11N} - X_{N00N})$ is positive definite and monotonically decreasing with N can be better understood by appealing to the fact that matrix elements of plane-wave operators appearing in this subsection are closely related to the real-space wavefunctions of Landau level states in the *symmetric* gauge, $\langle\vec{r}|N, m\rangle$. This momentum-position duality implies that the exchange energy

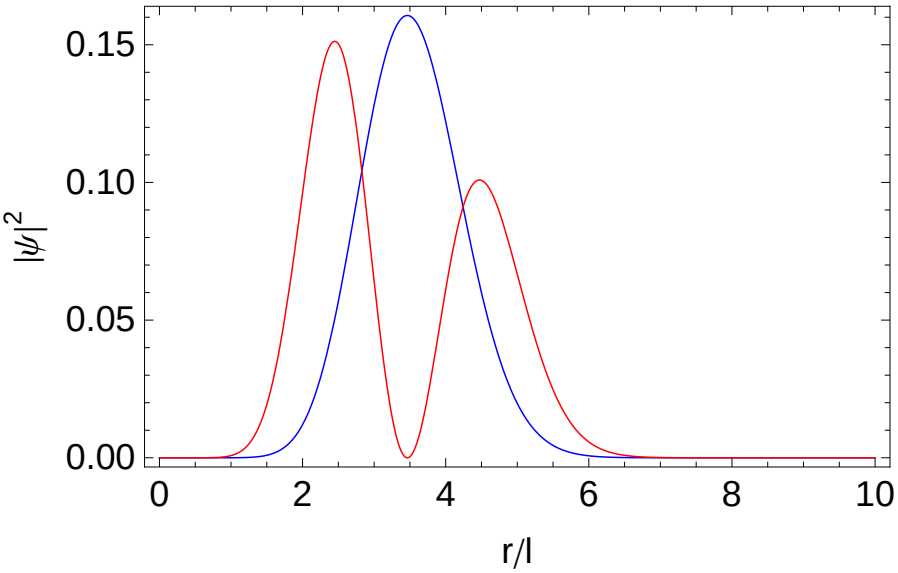

Figure 4.1: The contribution of Landau level N to the vacuum exchange energy of level n is the expectation value of the Coulomb potential $\frac{e^2}{r}$ with respect to the symmetric gauge state $|N, m = n\rangle$. Plotted is the squared modulus of the wavefunction versus radius in units of magnetic length. The blue curve corresponds to $|N = 6, n = 0\rangle$, the red to $|N = 6, n = 1\rangle$. The n=1 orbital experiences a stronger exchange potential since its wavefunction lies closer to the origin. The difference between $n = 0$ and $n = 1$ diminishes as N gets larger, since both wavefunctions get pushed farther from the origin.

difference due to a filled level N is actually just a difference in expectation value of the Coulomb potential (Fig 4.1) :

$$X_{N11N} - X_{N00N} = \langle N, 1|\frac{e^2}{r}|N, 1\rangle - \langle N, 0|\frac{e^2}{r}|N, 0\rangle \tag{4.21}$$

4.2.3 Modification of Vacuum Exchange by Inter-Layer Bias and Intrinsic Particle-Hole Asymmetry

Bilayer graphene is appealing as a subject of experimental and theoretical study in part because its electronic dynamics can be readily altered with a gate-induced inter-layer electric field. After incorporating an inter-layer potential difference in the four-band continuum model and renormalizing to the two-band model, one obtains the following single-particle Hamiltonian:

$$H = \omega_C \begin{pmatrix} 0 & a^2 \\ a^{\dagger 2} & 0 \end{pmatrix} + \xi U \left[\frac{1}{2} \begin{pmatrix} 1 & 0 \\ 0 & -1 \end{pmatrix} - \frac{\omega_C}{\gamma_1} \begin{pmatrix} aa^\dagger & 0 \\ 0 & -a^\dagger a \end{pmatrix} \right]. \tag{4.22}$$

The second term leads to an energetic difference between states of different valleys, while the third term generates a much smaller orbital splitting within in valley. The valence eigenstates of this Hamiltonian can be expresed in the general form of Eq(4.11) with coefficients $B_{-N}^{(U)}$ that depend on the bias potential U, the magnetic field strength, and the Landau level index N. Inter-layer biasing breaks particle-hole symmetry within a single valley, but the spectrum remains invariant under the combined operation of particle-hole conjugation and valley interchange. We use the analytic form of $B_{-N}^{(U)}$ (the expression is cumbersome and is not presented here) in the series expansion of Δ_{DS}, Eq(4.20), which we then evaluate numerically to determine the dependence of vacuum exchange on bias potential U. The results are presented in Figs 4.2 and 4.3. We find that in a range of magnetic field strengths depending on the magnitude of inter-layer bias, vacuum exchange generates a splitting between $n = 0$ and $n = 1$ orbitals that is significantly larger than the one present in the single-particle Hamiltonian.

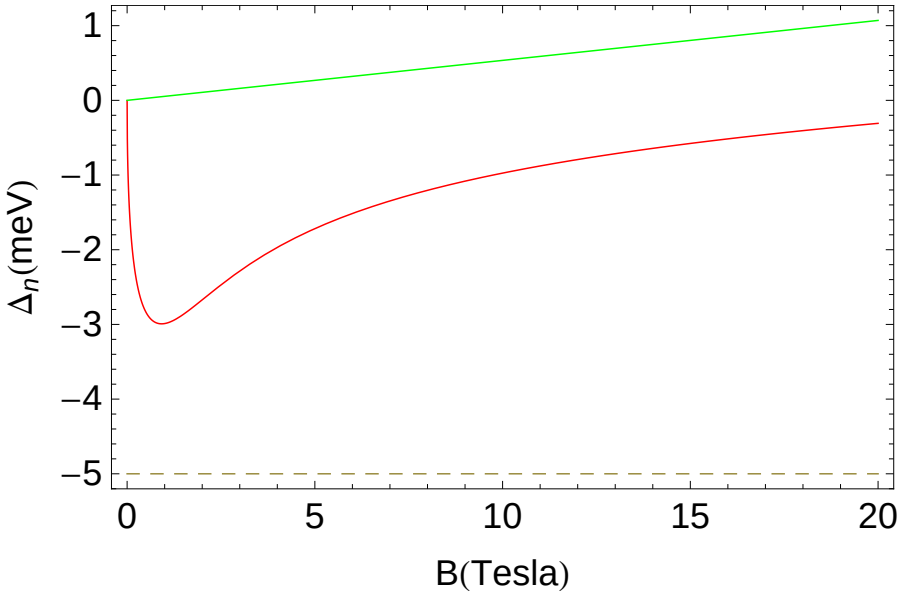

Figure 4.2: The effective single particle energy difference between n=1 and n=0 orbitals of the K-valley in meV, for an applied potential bias of 10meV. The usual contribution of the Dirac sea to orbital splitting is subtracted off ($\Delta^{(0)}_{DS} = -\frac{1}{8}\sqrt{\frac{\pi}{2}}\frac{e^2}{l_B}$) so that $\Delta_n = E_1 - E_0 - \Delta^{(0)}_{DS}$ and $\Delta_n = 0$ yields particle-hole symmetry. The purely single-particle contribution (green) is small relative to the vacuum exchange contribution (red), especially at weak magnetic field. The dashed line reminds us that the energies of both n=0 and n=1 electrons are reduced by 5meV, because K-valley states lie on the favorable layer. Layer-biasing breaks particle hole symmetry within one valley, but the spectrum remains invariant under the combined operation of particle-hole conjugation and valley-interchange (equivalent to spatial inversion in the LLL).

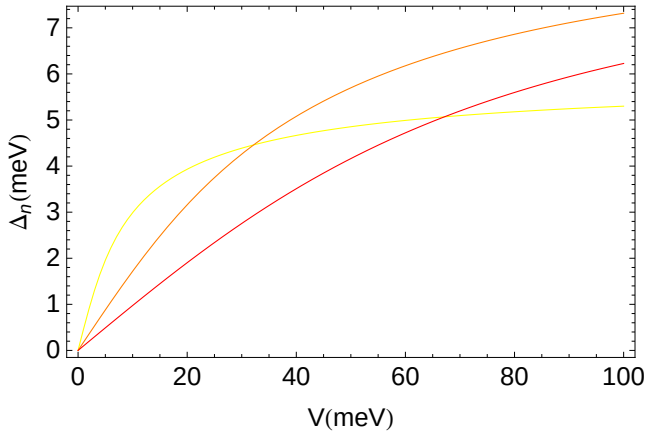

Figure 4.3: Vacuum-exchange contribution to orbital splitting for B=1,5,10 T (yellow,orange,red) as a function of the potential difference between layers.

Paralleling the calculation of the effect of biasing on vacuum exchange, we study the effect of band particle-hole asymmetry, captured by the Hamiltonian:

$$H = \omega_C \begin{pmatrix} 0 & a^2 \\ a^{\dagger 2} & 0 \end{pmatrix} + \Gamma\omega_C \begin{pmatrix} aa^\dagger & 0 \\ 0 & a^\dagger a \end{pmatrix} \tag{4.23}$$

A density functional theoretic calculation [41] reveals that non-nearest neighbor inter-layer hopping is the largest contributor to conduction-valence band asymmetry and suggests a value of $\Gamma \approx -0.1$. We find that in contrast to the case of layer-biasing, band particle-hole asymmetry does not significantly alter the eigenstates of BLG, and therefore does not appreciably modify the vacuum exchange potential (see Fig 4.4).

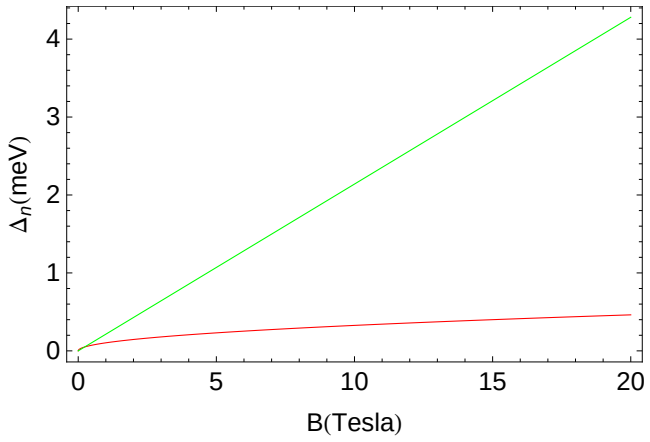

Figure 4.4: The vacuum-exchange contribution (red) to orbital-splitting is much smaller than the band contribution (green). Here, $\Gamma = -0.1$, corresponding to $\gamma_4 \approx 140$meV.

4.3 Mean-Field Solution of Single Flavor Model

Since the long-range Coulomb interaction is SU(4) spin-valley independent, the spectrum of quantum Hall ferromagnetic states of the lowest Landau level (corresponding to filling $\nu \in (-4, 4]$) can be simply constructed from the spectrum of the spinless, valleyless model. The single-flavor model retains the orbital degree of freedom and describes a range of filling, $\nu \in (0, 2]$. In this section we study the mean-field theory of the interacting single-flavor model including vacuum exchange, specified by:

$$H = \frac{1}{2}{\sum_{\alpha\beta\gamma\delta}}' v_{\alpha\beta\gamma\delta}\, c^\dagger_\alpha c^\dagger_\beta c_\gamma c_\delta + \frac{e^2}{\ell}\sum_X \left(\frac{3}{4}\sqrt{\frac{\pi}{2}}\, c^\dagger_{0,X} c_{0,X} + \frac{5}{8}\sqrt{\frac{\pi}{2}}\, c^\dagger_{1,X} c_{1,X}\right) \quad (4.24)$$

The Hartree-Fock decomposition of the interacting term is

$$V_{HF} = \frac{1}{N_\Phi}\frac{e^2}{\ell}\sum_{\alpha\beta\gamma\delta}{}'\sum_{\vec{q}}{}^{-} H_{n_\alpha n_\beta n_\gamma n_\delta}(\vec{q})\langle\rho_{n_\alpha n_\beta}(-\vec{q})\rangle\rho_{n_\gamma n_\delta}(\vec{q}) \\ - \frac{1}{N_\Phi}\frac{e^2}{\ell}\sum_{\alpha\beta\gamma\delta}{}'\sum_{\vec{q}} X_{n_\alpha n_\delta n_\gamma n_\beta}(\vec{q})\langle\rho_{n_\alpha n_\beta}(-\vec{q})\rangle\rho_{n_\gamma n_\delta}(\vec{q}), \quad (4.25)$$

where the overbar excludes summing over $\vec{q} = 0$, and both Hartree and Fock terms have been expressed in terms of the density operators

$$\rho_{n_\alpha n_\beta}(\vec{q}) = e^{-iq_x(X_\alpha + X_\beta)/2}\,\delta_{X_\alpha, X_\beta + q_y\ell^2}\, c^\dagger_{n_\alpha, X_\alpha} c_{n_\beta, X_\beta}. \quad (4.26)$$

The Hartree and Fock coefficients are:

$$H_{n_\alpha n_\beta n_\gamma n_\delta}(\vec{q}) = \frac{1}{q\ell} G_{n_\alpha n_\beta}(\vec{q}) G_{n_\gamma n_\delta}(-\vec{q}) \quad (4.27)$$

$$X_{n_\alpha n_\beta n_\gamma n_\delta}(\vec{q}) = \int \frac{d\vec{p}\ell^2}{2\pi} H_{n_\alpha n_\beta n_\gamma n_\delta}(\vec{p}) e^{i\vec{q}\times\vec{p}\ell^2}, \quad (4.28)$$

where $G_{n_\alpha n_\beta}(\vec{q})$ are the plane-wave matrix elements defined in Chapter 2 .

We assume homogeneous ground states, so $\rho_{n_\alpha n_\beta}(\vec{q}) = 0$ for $\vec{q} \neq 0$, therefore the Hartree terms vanishes. The relevant Fock coefficients are:

$$X_{0000}(0) = \sqrt{\frac{\pi}{2}} \quad (4.29)$$

$$X_{1111}(0) = \frac{3}{4}\sqrt{\frac{\pi}{2}} \quad (4.30)$$

$$X_{0110}(0) = X_{1001}(0) = \frac{1}{2}\sqrt{\frac{\pi}{2}} \quad (4.31)$$

$$X_{0011}(0) = X_{1100}(0) = \frac{1}{2}\sqrt{\frac{\pi}{2}} \quad (4.32)$$

For $\nu \leq 1$, electrons occupy only one Landau orbital psuedospinor, parameterized by

$$\psi_1 = z|0\rangle + \sqrt{1-|z|^2}|1\rangle \tag{4.33}$$

Then, the ground state energy is

$$E = -\frac{e^2}{\ell} \sum_{n_1,n_2,n_3,n_4} \frac{1}{2} X_{n_1,n_2,n_3,n_4} \langle \rho_{n_1,n_2} \rangle \langle \rho_{n_3 n_4} \rangle + \frac{e^2}{\ell} \sum_n \langle \rho_{nn} \rangle \left(\delta_{n,0} \frac{3}{4} \sqrt{\frac{\pi}{2}} + \delta_{n,1} \frac{5}{8} \sqrt{\frac{\pi}{2}} \right) \tag{4.34}$$

where the density matrices are

$$\langle \rho_{00} \rangle = \nu |z|^2 \tag{4.35}$$

$$\langle \rho_{11} \rangle = \nu (1-|z|^2) \tag{4.36}$$

$$\langle \rho_{01} \rangle = \nu \bar{z} \sqrt{1-|z|^2} \tag{4.37}$$

$$\langle \rho_{10} \rangle = \nu z \sqrt{1-|z|^2} \tag{4.38}$$

$$\tag{4.39}$$

We minimize the ground state energy with respect to z at fixed ν to obtain the ground state orbital-psuedospinor. A similar calculation follows for $1 < \nu \leq 2$, where ψ_1 is fully occupied and its orthogonal, $\psi_2 = \sqrt{1-|z|^2}|0\rangle - z|1\rangle$ is filled with $N_e = (\nu - 1)N_\phi \equiv \tilde{\nu} N_\Phi$ electrons. The density matrices in this case are

$$\langle \rho_{00} \rangle = \tilde{\nu} + |z|^2 (1-\tilde{\nu}) = \nu - 1 + |z|^2 (2-\nu) \tag{4.40}$$

$$\langle \rho_{11} \rangle = 1 - |z|^2 (1-\tilde{\nu}) = 1 - |z|^2 (2-\nu) \tag{4.41}$$

$$\langle \rho_{01} \rangle = \bar{z} \sqrt{1-|z|^2} (1-\tilde{\nu}) = \bar{z} \sqrt{1-|z|^2} (2-\nu) \tag{4.42}$$

$$\langle \rho_{10} \rangle = z \sqrt{1-|z|^2} (1-\tilde{\nu}) = z \sqrt{1-|z|^2} (2-\nu) \tag{4.43}$$

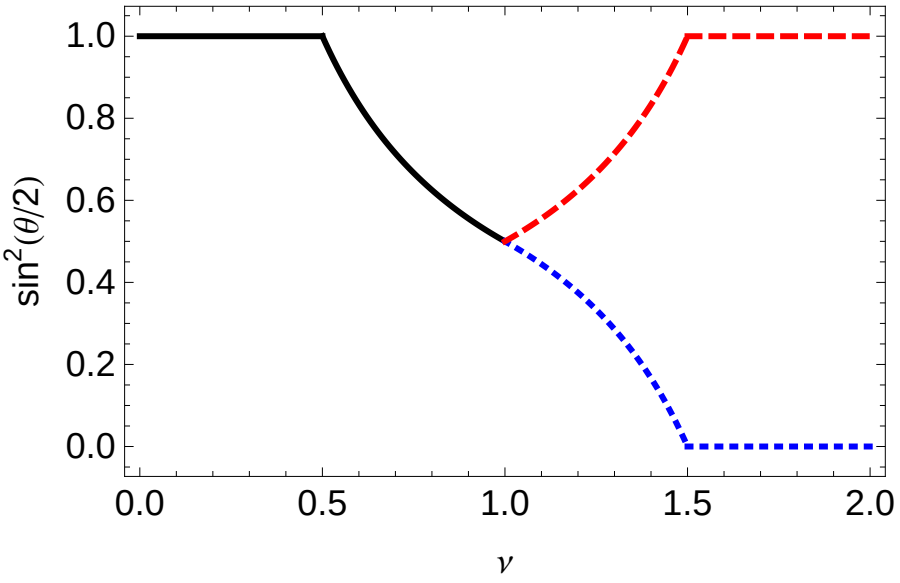

Figure 4.5: The HF ground state spinor/s as a function of filling. The y-axis plots the fraction of the spinor that is composed of the n=1 orbital. For $\nu \leq 1$ there is only one occupied spinor (solid black). For $\nu \leq \frac{1}{2}$ it is purely n=1. Above $\nu = \frac{1}{2}$ the ground state spinor is a coherent superposition of n=0 and 1, with equal weights at $\nu = 1$. Above $\nu = 1$, there is one completely occupied spinor (dotted blue) and one partially filled (dashed red). The solution is particle-hole symmetric, since adding electrons to the black spinor from the left is like adding holes to the red spinor from the right.

The orbital composition of the Hartree-Fock ground state and the ground state energy as a function of filling ν are presented in Figs 4.6 and 4.7.

4.4 Discussion

The results of this chapter suggest that if the particle-hole symmetry of bilayer graphene is preserved (as it might be, for example, in a suspended sample), mean-field states within the lowest Landau level will tend to display

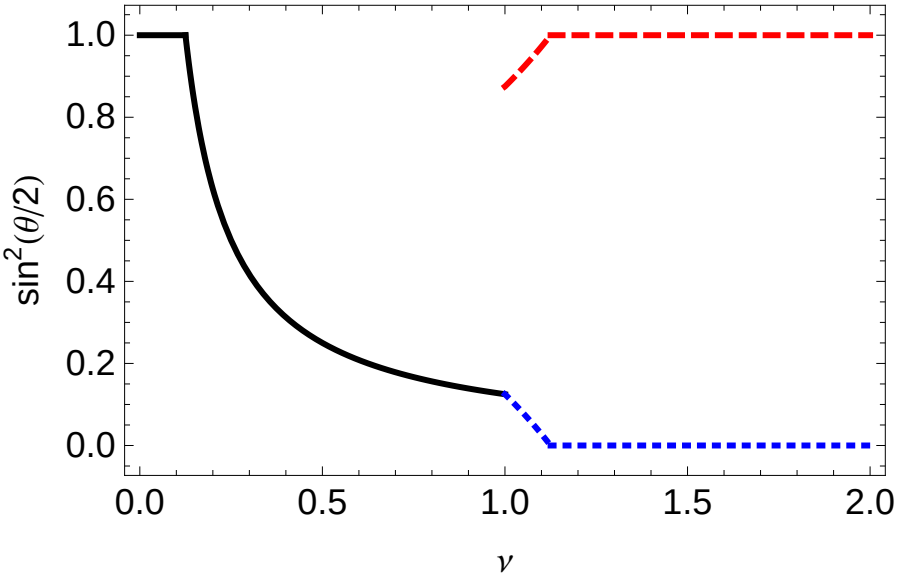

Figure 4.6: The HF ground state spinor/s as a function of filling, including substantial orbital splitting, $E_1 - E_0 = \frac{3}{32}\sqrt{\frac{\pi}{2}}\frac{e^2}{l_B}$. For $\nu \leq \frac{1}{8}$ the ground state is purely n=1. Above $\nu = \frac{9}{8}$ the fully occupied spinor is purely n=0. The solution is manifestly particle-hole asymmetric.

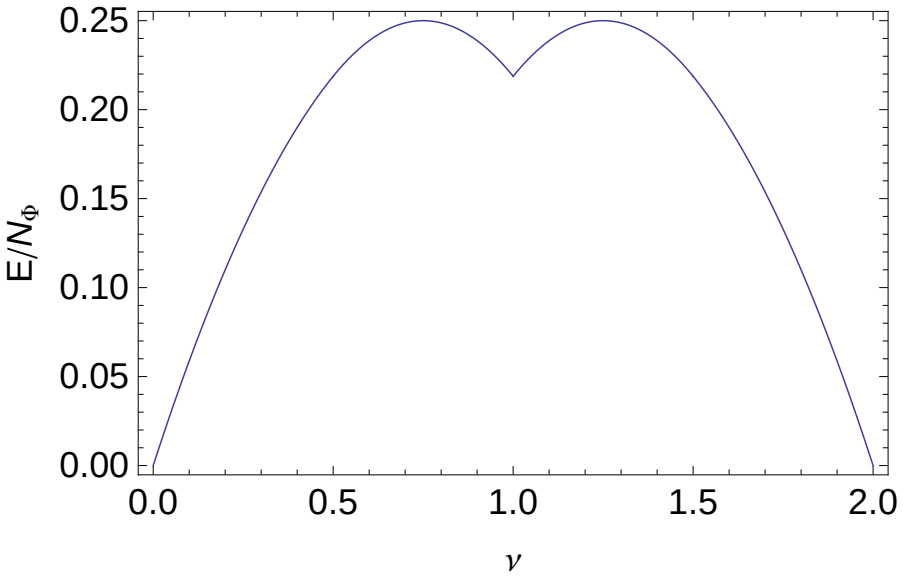

Figure 4.7: The ground state energy per flux quantum in units of $\sqrt{\frac{\pi}{2}}\frac{e^2}{l_B}$, as a function of filling.

coherence between $n = 0$ and $n = 1$ orbitals. We have shown that the orbital splitting in the presence of interlayer electric field can be substantially enhanced by exchange interaction with the Dirac sea. Inclusion of the Dirac sea interaction prompts further questions. How does vacuum exchange interplay with valley anisotropic contributions to the electron-electron interaction, to determine the nature of SU(4) symmetry breaking within the lowest Landau level? How are collective modes, in particular the mode related to a rotation between orbitals, altered by the effective orbital splitting resulting from vacuum exchange? Perhaps most interestingly, what is the spectrum of FQH states, and at what fractions are states most robust when there is a tendency towads orbital coherence?

Chapter 5

Conclusion

5.1 Summary

This thesis has explored the influence of disorder and interactions on the dynamics of electrons in bilayer graphene in a magnetic field using a low-energy two-band effective model, and the interaction physics of ABA-stacked trilayer graphene in the absence of a magnetic field using a six-band π-orbital model.

In Chapter 2, we observed that the spectrum of Landau levels lying close to the charge neutrality point of bilayer graphene depends sensitively on interlayer electric field. Incorporating disorder in the self-consistent Born approximation revealed that unbalancing the bilayer with an electric field leads to substantial alterations of the density of states. We found that the disorder-induced mixing of Landau levels, although unimportant beyond lowest order in the simple 2DEG, must be fully incorporated in order to derive the spectral functions of bilayer graphene's nearly degenerate $n = 0$ and $n = 1$ orbitals. Furthermore, disorder-mixing of particle and hole type states of higher ($|n| \geq 2$) levels must be included at any filling factor, at least to lowest order, in order to obtain the conductivity.

We found that the current operator is the sum of the usual term that induces transitions between neighboring Landau levels and an intra-Landau level term arising in the presence of an interlayer electric field. The *ac* conductivity reflected reflected these two types of transitions, and the structure of cyclotron resonance peaks was shown to depend substantially on interlayer electric field, and on filling.

The subject of study in Chapter 3 was the very peculiar case of ABA-stacked trilayer graphene, in which two of the four low-energy bands are monolayer-like, and two are bilayer-like. This partitioning of the Hamiltonian into disjoint monolayer and bilayer sectors is directly related to mirror-plane symmetry lattice symmetry and motivated a mean-field study of electronic interactions, with an emphasis on symmtery-breaking.

We found that at neutrality, interactions induce a transition from metal to insulator by reshaping and rearranging bands, but without breaking mirror-symmetry. Away from neutrality, principally on the hole-doped side, there appears a mirror-symmetry breaking metallic phase, in which electrons of a single spin-valley specie spontaneously polarize to one of the two extremal layers. In this case, mirror-symmetry breaking results in an avoided crossing between monolayer and bilayer type Hartree-Fock bands near the Fermi energy. We studied screening and found that in the presence of an interlayer electric field, electrons on one of the sublattices move in the field direction, while those on the other sublattice move oppositely.

In Chapter 4, we focused on interaction-induced quantum Hall ferro-

magnetic phases appearing in bilayer graphene's lowest Landau level. We emphasized the importance of the exchange potential generated by the infinite number of valence levels (the Dirac sea) on the dynamics of particles and hole states of the LLL. We discussed two ways of calculating this exchange potential, one an elegant regularization of the electron-electron interaction, the other a more general, brute-force approach. We studied the orbital character of the ground state, and its dependence on interlayer electric field and on a term that accounts for particle-hole asymmetry in bilayer graphene's bands.

5.2 Outlook

The three studies included in this thesis prompt additional questions and motivate further study.

Do beyond-mean-field correlation effects play a substantive role in the physics of disorder-free ABA-stacked trilayer graphene samples? Since experiments to date suggest that ABA graphene is metallic, it is reasonable to hypothesize that a calculation including screening may yield a different phase diagram. This hypothesis is reinforced from the theoretical side, by the fact that the metal-insulator transition onset occurs at finite coupling. A relatively simple extension of our study would include static screening of the inter-electron potential derived from the Lindhard function. This approximation could be invoked with or without self-consistency. Even if ABA graphene remains metallic in disorder-free, suspended samples, a remaining open question is whether screened interactions might allow for mirror-symmetry breaking

in the doped metal.

At present, there is much experimental and theoretical interest in bilayer graphene in the quantum Hall regime. A natural extension of the studies of Chapters 2 and 4 would combine disorder and electronic interactions commensurately. This could be done by evaluating the electron self-energy including the self-consistent Born approximation and the self-consistent Hartree-Fock potential. At fillings departing slightly from integers, disorder might pin skyrmion-like charged excitations.

An interesting open question concerns the structure and energetics of charged quasiparticles. It is likely that the nature of excitations within the lowest Landau level depends strongly on whether the filling is close to an odd or even integer. When the system is nearly particle-hole symmetric, as it may be in suspended samples, meron-like deformations of the psuedospin magnetization might appear near odd fillings when the ground state exhibits substantial orbital coherence. Elsewhere, charge-2e skyrmions or Laughlin-type quasiparticles might manifest.

Generally, the interplay of orbital-splitting and particle-hole asymmetry with interlayer electric field, magnetic field strength, valley anisotropic contributions to the electron-electron interaction, and filling factor suggests the possibility of a wide range of symmetry-breaking states near integer factors, and of novel correlated states at fractional fillings.

The simplicity and elegance of the effective models describing single and

multilayer graphene belie the systems' rich phenomenology and urges further study.

Bibliography

[1] A. H. Castro Neto, *et al.* "The electronic properties of graphene." Rev. Mod. Phys. **81**, 109–162 (2009). doi:10.1103/RevModPhys.81.109.

[2] R. Côté, *et al.* "Orbital and interlayer skyrmion crystals in bilayer graphene." Phys. Rev. B **82**, 245307 (2010). doi:10.1103/PhysRevB.82.245307.

[3] E. McCann and V. I. Fal'ko. "Landau-Level Degeneracy and Quantum Hall Effect in a Graphite Bilayer." Phys. Rev. Lett. **96**, 086805 (2006). doi:10.1103/PhysRevLett.96.086805.

[4] Y. Zhang, Y. Tan, H. Stormer, and P. Kim. "Experimental observation of the quantum Hall effect and Berry's phase in graphene." Nature **438**, 201–204 (2005). ISSN 0028-0836. doi:10.1038/nature04235.

[5] H. Min, G. Borghi, M. Polini, and A. H. MacDonald. "Pseudospin magnetism in graphene." Phys. Rev. B **77**, 041407 (2008). doi:10.1103/PhysRevB.77.041407.

[6] F. Zhang, H. Min, M. Polini, and A. H. MacDonald. "Spontaneous inversion symmetry breaking in graphene bilayers." Phys. Rev. B **81**, 041402 (2010). doi:10.1103/PhysRevB.81.041402.

[7] F. Zhang, *et al.* "Spontaneous Quantum Hall States in Chirally Stacked Few-Layer Graphene Systems." Phys. Rev. Lett. **106**, 156801 (2011). doi:10.1103/PhysRevLett.106.156801.

[8] D. J. Thouless, M. Kohmoto, M. P. Nightingale, and M. den Nijs. "Quantized Hall Conductance in a Two-Dimensional Periodic Potential." Phys. Rev. Lett. **49**, 405–408 (1982). doi:10.1103/PhysRevLett.49.405.

[9] Q. Niu, D. J. Thouless, and Y.-S. Wu. "Quantized Hall conductance as a topological invariant." Phys. Rev. B **31**, 3372–3377 (1985). doi: 10.1103/PhysRevB.31.3372.

[10] X. G. Wen. "Chiral Luttinger liquid and the edge excitations in the fractional quantum Hall states." Phys. Rev. B **41**, 12838–12844 (1990). doi:10.1103/PhysRevB.41.12838.

[11] X. G. Wen. "Theory of the edge states in fractional quantum Hall effects." International journal of modern physics B **06**, 1711–1762 (1992). doi:10.1142/S0217979292000840.

[12] Y. Hatsugai. "Chern number and edge states in the integer quantum Hall effect." Phys. Rev. Lett. **71**, 3697–3700 (1993). doi:10.1103/ PhysRevLett.71.3697.

[13] X. G. Wen and Q. Niu. "Ground-state degeneracy of the fractional quantum Hall states in the presence of a random potential and on high-

genus Riemann surfaces." Phys. Rev. B **41**, 9377–9396 (1990). doi: 10.1103/PhysRevB.41.9377.

[14] K. v. Klitzing, G. Dorda, and M. Pepper. "New Method for High-Accuracy Determination of the Fine-Structure Constant Based on Quantized Hall Resistance." Phys. Rev. Lett. **45**, 494–497 (1980). doi: 10.1103/PhysRevLett.45.494.

[15] J. Chalker and P. Coddington. "Percolation, quantum tunneling and the integer Hall-effect." Journal of Physics C **21**, 2665–2679 (1988). ISSN 0022-3719. doi:10.1088/0022-3719/21/14/008.

[16] A. H. MacDonald. "Introduction to the Physics of the Quantum Hall Regime." arXiv:cond-mat/9410047 (1994).

[17] T. Ando and Y. Uemura. "Theory of Quantum Transport in a Two-Dimensional Electron System under Magnetic Fields. I. Characteristics of Level Broadening and Transport under Strong Fields." J. Phys. Soc. Jpn. **36**, 959–967 (1974). doi:10.1143/JPSJ.36.959.

[18] D. Antoniou, A. H. MacDonald, and J. C. Swihart. "Collective oscillations in a disordered two-dimensional electron gas at strong magnetic fields." Phys. Rev. B **41**, 5440–5443 (1990). doi:10.1103/PhysRevB.41.5440.

[19] R. Nandkishore and L. Levitov. "Dynamical Screening and Excitonic Instability in Bilayer Graphene." Phys. Rev. Lett. **104**, 156803 (2010).

doi:10.1103/PhysRevLett.104.156803.

[20] F. Zhang and A. H. MacDonald. "Distinguishing Spontaneous Quantum Hall States in Bilayer Graphene." Phys. Rev. Lett. **108**, 186804 (2012). doi:10.1103/PhysRevLett.108.186804.

[21] M. Koshino and E. McCann. "Gate-induced interlayer asymmetry in ABA-stacked trilayer graphene." Phys. Rev. B **79**, 125443 (2009). doi:10.1103/PhysRevB.79.125443.

[22] J. Jung, *et al.* unpublished .

[23] T. Morimoto and M. Koshino. "Gate-induced Dirac cones in multilayer graphenes." Phys. Rev. B **87**, 085424 (2013). doi:10.1103/PhysRevB.87.085424.

[24] M. Serbyn and D. A. Abanin. "New Dirac points and multiple Landau level crossings in biased trilayer graphene." Phys. Rev. B **87**, 115422 (2013). doi:10.1103/PhysRevB.87.115422.

[25] T. Taychatanapat, K. Watanabe, T. Taniguchi, and P. Jarillo-Herrero. "Quantum Hall effect and Landau-level crossing of Dirac fermions in trilayer graphene." Nat. Phys. **7**, 621–625 (2011). doi:10.1038/nphys2008.

[26] W. Bao, *et al.* "Stacking-dependent band gap and quantum transport in trilayer graphene." Nat. Phys. **7**, 948–952 (2011). doi:10.1038/nphys2103.

[27] D. C. Tsui, H. L. Stormer, and A. C. Gossard. "Two-Dimensional Magnetotransport in the Extreme Quantum Limit." Phys. Rev. Lett. **48**, 1559–1562 (1982). doi:10.1103/PhysRevLett.48.1559.

[28] R. B. Laughlin. "Anomalous Quantum Hall Effect: An Incompressible Quantum Fluid with Fractionally Charged Excitations." Phys. Rev. Lett. **50**, 1395–1398 (1983). doi:10.1103/PhysRevLett.50.1395.

[29] S. L. Sondhi, A. Karlhede, S. A. Kivelson, and E. H. Rezayi. "Skyrmions and the crossover from the integer to fractional quantum Hall effect at small Zeeman energies." Phys. Rev. B **47**, 16419–16426 (1993). doi:10.1103/PhysRevB.47.16419.

[30] A. Usher, R. J. Nicholas, J. J. Harris, and C. T. Foxon. "Observation of magnetic excitons and spin waves in activation studies of a two-dimensional electron gas." Phys. Rev. B **41**, 1129–1134 (1990). doi:10.1103/PhysRevB.41.1129.

[31] H. A. Fertig, L. Brey, R. Côté, and A. H. MacDonald. "Charged spin-texture excitations and the Hartree-Fock approximation in the quantum Hall effect." Phys. Rev. B **50**, 11018–11021 (1994). doi:10.1103/PhysRevB.50.11018.

[32] H. A. Fertig, *et al.* "Hartree-Fock theory of Skyrmions in quantum Hall ferromagnets." Phys. Rev. B **55**, 10671–10680 (1997). doi:10.1103/PhysRevB.55.10671.

[33] J. P. Eisenstein and A. H. MacDonald. "Bose-Einstein condensation of excitons in bilayer electron systems." Nature **432**, 691–694 (2004). doi:10.1038/nature03081.

[34] K. Moon, *et al.* "Spontaneous interlayer coherence in double-layer quantum Hall systems: Charged vortices and Kosterlitz-Thouless phase transitions." Phys. Rev. B **51**, 5138–5170 (1995). doi:10.1103/PhysRevB.51.5138.

[35] D. Nandi, *et al.* "Exciton condensation and perfect Coulomb drag." Nature **488**, 481–484 (2012). doi:10.1038/nature11302.

[36] D. A. Abanin, B. E. Feldman, A. Yacoby, and B. I. Halperin. "Fractional and integer quantum Hall effects in the zeroth Landau level in graphene." Phys. Rev. B **88**, 115407 (2013). doi:10.1103/PhysRevB.88.115407.

[37] M. Kharitonov. "Phase diagram for the $\nu = 0$ quantum Hall state in monolayer graphene." Phys. Rev. B **85**, 155439 (2012). doi:10.1103/PhysRevB.85.155439.

[38] I. Sodemann and A. H. MacDonald. "Broken SU(4) Symmetry and The Fractional Quantum Hall Effect in Graphene." doi:arxiv/1310.1642.

[39] K. Shizuya. "Structure and the Lamb-shift-like quantum splitting of the pseudo-zero-mode Landau levels in bilayer graphene." Phys. Rev. B **86**, 045431 (2012). doi:10.1103/PhysRevB.86.045431.

[40] K. Shizuya. "Orbital Lamb shift and mixing of the pseudo-zero-mode Landau levels in ABC-stacked trilayer graphene." Phys. Rev. B **87**, 085413 (2013). doi:10.1103/PhysRevB.87.085413.

[41] I. Sodemann and A. H. MacDonald. "Accurate tight-binding and continuum models for the π bands of bilayer graphene." doi:arxiv/1309.5429.

[42] P. Maher, *et al.* "Evidence for a spin phase transition at charge neutrality in bilayer graphene." Nature Physics **9**, 154–158 (2013). ISSN 1745-2473.

[43] M. Kharitonov. "Canted Antiferromagnetic Phase of the ν=0 Quantum Hall State in Bilayer Graphene." Phys. Rev. Lett. **109**, 046803 (2012). doi:10.1103/PhysRevLett.109.046803.

[44] E. A. Henriksen, D. Nandi, and J. P. Eisenstein. "Quantum Hall Effect and Semimetallic Behavior of Dual-Gated ABA-Stacked Trilayer Graphene." Phys. Rev. X **2**, 011004 (2012). doi:10.1103/PhysRevX.2.011004.

[45] I. B. Spielman, J. P. Eisenstein, L. N. Pfeiffer, and K. W. West. "Resonantly Enhanced Tunneling in a Double Layer Quantum Hall Ferromagnet." Phys. Rev. Lett. **84**, 5808–5811 (2000). doi:10.1103/PhysRevLett.84.5808.

[46] S. Girvin. "The quantum hall effect: Novel excitations and broken symmetries." In Comtet, A and Jolicoeur, T and Ouvry, S and David, F (Ed.), *TOPOLOGICAL ASPECTS OF LOW DIMENSIONAL SYSTEMS*, volume 69 of *LES HOUCHES SUMMER SCHOOL SESSION*,

pp. 53–175 (NATO, Adv Study Inst; Univ Joseph Fourier Grenoble; Ecole Phys Houches; Inst Nucl Phys Grenoble; Minist Educ Natl Rech Technol; CNRS; CEA; Natl Sci Fdn, 2000). ISBN 3-540-66909-4. ISSN 0924-8099. Les Houches Session LXIX on Topological Aspects of Low Dimensional Systems, NATO, ADV STUDY INST, LES HOUCHES, FRANCE, JUL 07, 1998-JUL 31, 1999.

[47] C. H. Lui, *et al.* "Observation of an electrically tunable band gap in trilayer graphene." Nat. Phys. **7**, 944–947 (2011). doi:10.1038/nphys2102.

[48] T. Ando, A. B. Fowler, and F. Stern. "Electronic properties of two-dimensional systems." Rev. Mod. Phys. **54**, 437–672 (1982). doi:10.1103/RevModPhys.54.437.

[49] J. Jung and A. H. MacDonald. "Gapped broken symmetry states in ABC-stacked trilayer graphene." Phys. Rev. B **88**, 075408 (2013). doi:10.1103/PhysRevB.88.075408.

Vita

Rohit Hegde was born in the town of Stony Brook, New York in 1984. He received a Sc.B. degree in Physics from Brown University in 2005, and worked for one year at the Indian Institute of Science in Bangalore before commencing graduate study at the University of Texas, Austin.

Permanent address: rohegde@gmail.com

This dissertation was typeset with LaTeX[†] by the author.

[†]LaTeX is a document preparation system developed by Leslie Lamport as a special version of Donald Knuth's TeX Program.